ANALYSIS OF CENTRIFUGE PILE TESTS; SIMULATION OF PILE-DRIVING

Ronald F. Scott

Report Through September 30, 1979
Research Program

for

American Petroleum Institute
OSAPR Project 13

February 20, 1980
Revised June 20, 1980

Soil Mechanics Laboratory
Division of Engineering and Applied Science
California Institute of Technology
Pasadena, California 91125

INTRODUCTION

Previous studies on the centrifuge have been directed towards simulating the behavior of a laterally-loaded pile in fine, dry and saturated sand. After data had been obtained on the model pile, attention was turned to modelling the soil-pile interaction behavior. Since the Winkler [continuous reaction elements (springs) distributed along the pile length] foundation representation is the simplest that can be adduced, and, moreover, has been found to give adequate results for design in a variety of foundation problems, attempts were made to extract a Winkler type of function from the model pile test results.

The pile response is obtained from the output of a series of strain gauges attached to the pile. In effect these indicate the bending moment in the pile as a function of length along it. As a consequence, to obtain the pile-soil interaction behavior at various locations along the pile, it is necessary to integrate the bending moment function twice for each level of applied load to obtain pile displacements (the top displacement is measured and known), and to differentiate it twice, to get the soil interaction pressure. Then, at a given point on the pile, the pile-soil interaction behavior is given by plotting the pressure versus the displacement at various load levels. A series of such functions at different depths gives the information required for subsequent analyses.

The troubles with this procedure are well-known. Double integration is satisfactory and gives a good indication of pile deflections, since the smoothing process eliminates the effect of random errors in the measurement of pile strains. However, double differentiation exaggerates the same errors, and the resulting pressure function can be quite erratic. It is

necessary to smooth the strain gauge data first before processing it; various smoothing techniques are available and have been tried. The results of preliminary attempts at obtaining a smoothing function are described in a previous report (3).

In the stage of the work reported here, a revised method of analysis was developed, and applied both to calibration tests of the pile, and to the tests carried out in dry and saturated sand. The results of these applications are described below.

TESTS AND REVISED ANALYSIS

Rubber Winkler Foundation

The sequence of calculations leading from loaded pile in the centrifuge to soil interaction pressure versus displacement at a particular depth in the soil is so tortuous that a determination of the precision of the final relationship was deemed necessary. It was decided to do this by imbedding and testing the pile in an array of linearly elastic supports of known properties. The initial attempt involved construction of a multiple steel cantilever beam support system for the pile. A Winkler foundation would be approximately represented by the flexible cantilevers. Difficulties were encountered in attaching the cantilevers to the pile without interfering with the strain gauges, in supplying enough closely-spaced cantilevers to represent the Winkler system adequately, and in arriving at the right stiffness for the beams, approximately to represent the soil restraint. After a few trials, this system was abandoned for a simpler arrangement.

It should be pointed out that it is not a good solution to completely imbed the pile in a rubber or other polymer medium (this could relatively easily be contrived), because the solution to the problem of a laterally-loaded pile in a linearly-elastic medium has not been obtained. In consequence, the derived soil pressure-displacement function would lack basis for confirmation, which the Winkler solution provides. A different approach to constructing a Winkler support for the pile was therefore devised.

Test Arrangement

In other current tests in a different research area in the laboratory a very stiff rubber was being used. It was decided to employ this, as it is the correct order of stiffness and is reasonalby linear in its

properties over the pressure range required. Two strips of this rubber, 0.25 inch square in cross section and the same length as the model pile, were cut out. The width, 0.25 inch, was the same as that of the model pile.

At 0.25 inch intervals down each strip, slots, about 0.02 inch wide, were incised, to leave each strip crenellated. A sufficient thickness of base, also about 0.02 inch, was left to secure the 0.25 inch cube rubber blocks to one another. The pile was sandwiched between the two strips, which were bonded at the continuous base to two aluminum base plates. The base plates, in turn, were backed up by steel channels, to insure that the base level of the rubber strips could be considered truly rigid. Thus, in effect, the pile was supported on both sides by a row of 0.25 inch cubes of stiff rubber, with enough spacing between the rubber blocks for them to act independently of each other. The arrangement is illustrated in Figure 1. Within the limits of the reversibility and linearity of the rubber, the pile was then embedded in a Winkler foundation, but only approximately, since the blocks were finite in size. Some prestress was applied to the rubber blocks by clamping the channels on each side of the pile, so that the pile would not lift off anywhere, upon loading.

When the pile was originally instrumented with strain gauges, they were covered with a polymer coating to render them waterproof. This coating was dissolved off before the rubber block test, so that its properties would not be reflected in the experiment. With the arrangement shown in Figure 1, the pile was tested by a lateral load hung on a string passing through the small hole in the pile at the original loading point. The displacement at this point on loading was also measured. Both load and displacement were measured with the same transducers as employed in the

centrifuge soil tests, and the signals were passed through the same amplifiers and slip rings to the same recorder. Strains (which correspond to moments) were indicated by the same six strain gauges on the pile as formerly, with the exception of one gauge which became partially detached during the polymer solution process and had to be replaced. The replacement is the same size and make, and possesses the same calibration factor as the other gauges. The strain gauges were calibrated in the same way as before, by hanging a weight on the end of the pile supported as a pure cantilever and recording the trace displacements on the recorder after they passed through the centrifuge system. This weight gave rise to known moments at the gauge locations on the pile. Only very small changes in the gauge calibrations had occurred since the first soil tests with the model pile a year before.

Results

The gauge records from the rubber "Winkler" tests were digitized for computer processing the same way as formerly. When the strain gauge readings, converted to prototype moment* form, were plotted as functions of depth at various load levels, they were much less smooth either than expected or than the values obtained from the previous soil tests. The soil test results at each load level had exhibited such a smoothly-varying function with depth that they had suggested the spline fitting technique

---

*It was assumed, for convenience, that the rubber Winkler test, actually performed at 1g, was also a 1/100 scale test, just as in the case of the soil experiments. All the test results were therefore expressed as before, in terms of prototype dimensions. This facilitates comparison with the soil tests. Since the rubber properties are essentially independent of stress, the rubber support test would have behaved the same had it been conducted at 100g.

described previously (3). The variations in the Winkler test indicated that a recheck of the strain gauge calibrations and their performance was necessary. A number of independent tests of their behavior all suggested that they were behaving correctly and that the slightly erratic results were an inherent test characteristic, reflecting small variations in the compressibility of the rubber blocks, temperature variations, and other unknown factors.

It was therefore not possible to fit these results with spline functions in any direct way that would give appropriate soil pressure-depth relations from two differentiations. Figure 2 shows the consequences of applying this technique to a rubber Winkler test. It can be seen that the slightly irregular nature of the moment-depth data drives the spline functions into sinuations whose first and second derivatives exhibit increasing complexity. The result is, of course, that the pressure distribution [Figure 2(c)] which, in this case, is expected to have the same shape as the deflected curve of the pile, is completely erroneous. No manipulation of the spline technique, for example, by variation of the point of zero moment, as was done previously, has any significant effect on the pressure distribution. No useful information, in this analysis, can be extracted from the soil pressure-displacement traces, Figure 2(f), even though, as usual, the process of repeated integration gives reasonable displacements, Figure 2(d).

The significance of this result was that the errors in the strain gauge (moment) readings were larger than was thought to be the case. It was apparent that the same errors should be considered to be inherent in the soil test data also, and that the information deduced from the pressure-displacement plots of these tests was probably not reliable.

Another analysis, properly accounting for the erratic nature of the moment data, was therefore sought. The next section describes the revised analysis technique.

Revised Analysis Method

Usually, plots of data points such as strain gauge (moment) results from the pile tests are fitted by a polynomial using a least squares analysis. The polynomial, unlike the spline fit, does not pass through all data points, but instead provides a smooth averaged fit to the information. Indeed, as described previously (3), polynomial functions were examined in preliminary studies of the soil test data, but were rejected partly because of various inconvenient features in their use, but mostly because the spline functions apparently described the test points so well.

As they are commonly applied, polynomial curves treat the zero moment at the top of the pile (at the loading point) and the zero moment ascribed to the bottom of the pile (or at an arbitrarily higher position) as two other data points that help constrain the coefficients of the polynomial, but through which the polynomial curve need not necessarily pass. In addition, there is generally no contraint placed on the derivatives of the polynomial function at top and bottom of the pile. The first polynomial fitting attempt (3) followed these conditions but has now been modified, as follows. At the top, in the present case, the first derivative is equal to the applied load; at the pile tip, or at some arbitrary point sufficiently far down the pile, the displacement, slope, moment, shear and net soil interaction pressure are all zero. Also at the top of the pile, there are some other conditions depending on the medium of imbedment. In dry or saturated sand, the soil interaction pressure at ground surface (in the

tests here, this corresponds to the load application point, also) is zero. In an overconsolidated clay or in a Winkler-acting medium of unknown properties the pressure at the ground surface is unknown, on the other hand. Finally, at ground surface, in the tests in question, displacement is also measured. Some of these known quantities can be used to limit the variations in the fitting function; they were so used with the spline technique. In view of the apparent errors in the test data, it was decided to re-examine the polynomial fitting approach.

In the case of a polynomial, the first consideration is its order. Since two differentiations are to be performed on it, and the result of the second of these is expected to be a smoothly-varying function with depth, it is obvious that the moment polynomial cannot have order lower than 5. Its value was therefore selected to be 5 for simplicity. Thus, the polynomial is required to have the form

$$M = az^5 + bz^4 + cz^3 + dz^2 + ez + f \qquad (1)$$

to fit the experimental moment (M) points as a function of depth, z. In all the pile tests, the moment at the pile top (z = 0) was zero, which requires the constant f to be zero. Since the first derivative is equal to the load at z = 0, it follows that e must be made equal to the applied load. In the case of the second derivative, it may be zero in the case of sand, at z = 0, so that d = 0, or unspecified, and therefore to be determined by the fitting process at this level, in the Winkler or other soil cases. At the ground surface it is not apparent how the known displacement (equalling 1/EI times the second integral of moment) can be used to constrain the polynomial, so this condition was left to be used as a check on the computations. No constraint was placed on the polynomial behavior

at depth; only the six data points and the top conditions described above were used. As a consequence the polynomial cannot be used to describe pile bending much below the lowest strain gauge. This region has to be accounted for in a different way. Thus, when fitting was accomplished for the data points at each load level, the polynomial was evaluated at the level of each strain gauge, and these smoothed values were then taken as input to the previous spline-fitting technique. The last spline segment was constrained by the same requirement as before, namely, that the moment, slope and second derivative were all zero at a point located at an arbitrary distance below the deepest strain gauge on the pile. As before, this point was obtained by inspection of the moment behavior to be separated from the last data point by twice the interval between the strain gauges above.

With polynomial smoothing and spline-fitting accomplished for each applied load, the double integration and differentiation proceeded as before, in the case of the rubber-block Winkler medium. Finally, the calculated interaction pressure was plotted versus the calculated displacement at various levels down the model pile. The results are displayed in Figure 3. It can be seen from Figure 3(d) that the relation pressure/displacement is close to linear, and nearly the same for all points on the pile. Since the rubber block response is constant, and independent of position, this is as it should be. Also plotted on Figure 3(d) is the result of an independent test performed on a pair of rubber blocks in the absence of the pile. Their behavior appears to correspond well with that deduced from the complicated pile-soil interaction described by the strain gauge records. The rubber exhibits some hysteresis in both tests since it possesses internal damping. Another rubber block test was performed in which the rubber was compressed somewhat more around the model pile. Since the rubber

stiffens on compression, the result was a steeper slope to the deduced pressure/displacement curves. They are shown on Figure 3(e) along with the results of another independent direct rubber block test at a higher level of prestress in the blocks.

It can be concluded, therefore, that the combined polynomial/spline fitting technique describes the behavior of the imbedded pile under bending loads as well as can be attained. This fitting procedure was then applied to the previous tests of lateral loading applied to the pile imbedded in both dry and saturated sands.

Revised Analyses of Pile Lateral Load Tests

As part of the initial smoothing procedure, equation (1) was used to describe the strain gauge readings for the previous tests performed on piles imbedded in dry and saturated Nevada sand. For both the sand test series, the coefficients d and f were made equal to zero, and coefficient e was taken as the lateral load acting at the top of the pile, according to the argument presented previously. From the polynomial fit, data points were obtained for the subsequent spline application. When the spline coefficients had been determined, the double integrations and differentiations were performed to give eventually the interaction pressure versus displacement curves at several depths below the soil surface. The results are shown in Figures 4 and 5 for dry and wet sand tests respectively. The curves, in order, refer to behavior at prototype depths of 8, 25, 50, 75, 100, 125 and 150 inches.

It can immediately be seen from Figures 4(a) and 5(a) that many of the objectionable features in the previous analysis (3) have been removed. The soil response changes progresively with depth, becoming stiffer with

depth. In previous analyses, some of the curves at different depths crossed each other. It now appears that the data are in reasonable shape, and that interpretation of the soil/pile response can proceed with greater confidence than before. Figures 4(b) and 5(b) are included to show the consistent behavior of the second cycle of load and unload. The second load curves in those figures all begin from the corresponding points in Figures 4(a) and 5(a) at the end of the first unloading stage.

Only the initial pressure-displacement behavior in Figures 4(a) and 5(a) is now possibly questionable. All the curves are seen to exhibit extremely steep ascents at small loads, implying a stiff soil response and only a small range of elastic behavior. If the simple bilinear model suggested in a previous report is adhered to, then it is desirable to obtain the initial linearly elastic behavior from the slope of the unloading portion of each curve. This has been done and these slopes are plotted as a function of soil depth in both dry and saturated sand in Figure 6, which is drawn similarly to Figure 12 of the previous report (3) with changes indicated in the caption. The revised fitting procedure gives rise to a soil/pile interaction stiffness which increases as a function of vertical effective stress (or depth) in a fashion much more nearly linear than before. The values from the saturated test are also shown in Table 1.

When the plastic stiffness (the slope of the second straight line segment at each depth) is plotted in the diagram, a relation close to linear is also observed. The plastic stiffness is approximately one quarter of the elastic value. To obtain an analytical description of this behavior, the model discussed in the Appendix was investigated; it represents an improvement on the previous construction (3). From this Appendix, two features of interest can be obtained: the elastic pile force-displacement

relation, and the interaction force at which the soil yields. It can be seen from Figure A.2 that the soil/pile stiffness depends on the soil's Poisson ratio and, more strongly, on the ratio assumed for the radii (or diameter) of the pile and affected region of soil. In general, the Poisson ratio can be taken to be about 0.3 for a medium-dense sand, and up to 0.5 for a saturated, undrained clay. It is often considered, although on the basis of very skimpy evidence, that piles placed at distances of 8 or 10 diameters from each other undergo little or no interaction under lateral loads. If this can be taken as correct, it indicates that a single pile's behavior can be deduced from the curves in the appendix if the radius ratio is taken to be, say, 10. With a radius ratio of 10, and the above values of Poisson's ratio, it can be seen from Figure A.2 that the pile/soil stiffness lies in the range 0.8 to 1.2 times E, the elastic modulus of the soil. Since it is easy to remember, it is suggested that the stiffness/modulus be taken as unity. In this case, the elastic coefficient points of Figure 6, and the "elastic" slope values in Table 1 also represent the Young's modulus of the soil at various depths or confining pressures.

At the initiation of plasticity in a simple Von Mises model of clay yielding at shear stress c (Poisson's ratio = 0.5) (cohesion), it is found that yielding commences at the circular pile surface on the ends of the diameter transverse to the loading direction. The end of linearly elastic behavior, or the commencement of plasticity, occurs when the pile force (per unit length) F reaches the value

$$F = 2\pi ac \qquad (2)$$

In the case of cohesionless material, plastic development is more complicated, and depends on the friction angle of the material, as well as Poisson's ratio. Yielding begins at points on the circumference of the pile behind the transverse diameter (the front of the pile is where the soil is being compressed by the pile's movement); the angle to the yield initiation spot depends on Poisson's ratio and the friction angle. Figure A.10 shows the relation between these quantities, the overburden pressure and the force F required to cause yielding. The development of plasticity in the soil is still being studied and will be discussed in more detail in a later report.

Comparison of Results with API Method

A method of determining the lateral resistance versus deflection (the "p-y" curve) for a pile imbedded in sand is outlined in the API document RP2A (1) based on the results of two full-scale pile tests by Reese, et al. (2). It is of interest to calculate the figures which the API method would give for the centrifuge pile tests in saturated sand.

The API technique describes the lateral load-deflection relation for a pile by a curve which exhibits first a straight line portion (linearly elastic) to deflection y_k, reaction force p_k, then a parabolic (yielding) section to (y_m,p_m), and a straight line segment again to (y_u,p_u), after which the soil around the pile is considered to have failed and deflects at constant force p_u. The guide RP2A gives equations and tables for determining the various values of y and p.

For saturated sands a table in RP2A gives an elastic subgrade reaction coefficient (k_1 in table) for loose, medium, and dense relative densities. When k_1 is multiplied by the depth, the resulting coefficient can be

compared with the slopes estimated from the centrifuge pile analysis for saturated sand, as shown in Figure 5. The following table gives the results for saturated sand.

Table 1

Depth, inches	Vertical Effective Stress, psi	"Elastic" slope, psi	"Plastic" slope, psi	"Elastic" Values from RP2A		
				Loose k_1 20 pci	Medium k_1 60 pci	Dense k_1 125 pci
8	0.277	160	70	160	480	1,000
25	0.865	590	233	500	1500	3,100
50	1.730	1147	470	1000	3000	6,250
75	2.595	1800	745	1500	4500	9,300
100	3.461	2550	990	2000	6000	12,500
125	4.326	3400	1220	2500	7500	15,600
150	5.191	4500	1420	3000	9000	18,800

A comparison between columns 3 and 5, 6, or 7 indicates that the soil in the centrifuge test would be classified as a little denser than "loose." It would correspond to a value of k_1 in RP2A of about 25 pci (based on 100 inch depth figures). Such a value would correspond to a soil friction angle ϕ of about 32^{o}, which will be used in subsequent analyses. From Figure 6 it is apparent that the dry sand "elastic" values closely follow those for the saturated sand, so that the same conclusions hold.

Since the soil in the centrifuge tests on which Table 1 is based was prepared with some compaction, it had been considered to be in a medium dense rather than loose condition. Thus the relatively close similarity

of the test "elastic" values with the RP2A "loose" values is surprising. There may be several reasons for this result.

First, the RP2A figures are based on full-scale pile tests in a natural saturated sand deposit, whereas the centrifuge tests were carried out in a remolded soil prepared in the laboratory. There is good reason to suspect that a natural soil at a site where it was deposited hundreds to thousands of years (or longer) ago will be stiffer than a laboratory soil of the same grain size distribution at the same unit weight or void ratio. The difference may be due to a slight cementation which develops in natural soils, or due to grain rearrangements which take place over the course of time, changing the structure or fabric of the natural material without altering the overall void ratio significantly.

Second, a full-scale pile is usually driven with a closed end, or, if it is driven open-ended, the incoming soil eventually forms a plug which effectively closes the end. In either case, the soil along the axis of the pile's movement is displaced radially by the pile, compressing the material in the vicinity of the pile. The resulting increase in unit weight is a local effect, giving rise to increased frictional resistance along the pile, and also to an increase in lateral resistance. Investigatory borings at the pile site do not, of course, detect this increase in unit weight and stiffness. Pile-driving vibrations also play a part in raising the local unit weight. Thus a natural soil, which would be characterized as "loose" or "medium-dense" in pre-pile site investigations, will give a lateral pile resistance higher than that which would be directly associated with the overall site characteristics.

In the centrifuge, apparatus limitations require the model pile to be installed in the soil at 1g, either by pushing into the soil, which

would presumably result in small local density increases (but not the same as those which would be obtained by insertion at 100g) or, in the case of the tests in the medium-dense laboratory soil, by installing the pile in the empty test chamber at 1g and compacting the soil around it. In neither case is the pile driven by impact. In the latter circumstance the soil is not denser in the pile vicinity, and may even be somewhat looser on the average close to the pile because of the difficulty of compacting beside the pile. For the tests discussed here, the pile was inserted by pushing it into the soil at 1g. By both of the above arguments, the soil next to the pile in the centrifuge model will be less stiff than a similar natural soil at about the same unit weight in a full-scale field test.

The value of deflection y_u at which the ultimate reaction load p_u occurs in the RP2A is 0.9" (3D/80 where D is pile diameter) independent of depth; this value is higher than any deflections recorded in the centrifuge tests, and therefore confirms, tentatively, the observation from Figures 4 and 5 that an ultimate reaction load was not reached in the centrifuge tests. At the intermediate point (y_m,p_m) however, the force is given as a ratio Bp_u/A where B and A are two experimentally-determined constants (functions of depth) given in RP2A. Consequently, although its value was not reached in the centrifuge tests, p_u must be calculated for comparison purposes. The value of y_m is given as D/60, again independent of depth, so that for the 24 inch diameter pile of the tests, that deflection is 0.4 inches which falls within the range of centrifuge test values. The initial slope of the curve from the origin is already given for each depth by the value selected from Table 1 and this straight line terminates at the point (y_k,p_k) in which y_k is given by an expression in RP2A involving

the empirical constants A and B and p_m. The terminal linear reaction force, p_k, is related linearly to y_k at each depth by the stiffness.

The constants A and B are given in the form of plotted curves in RP2A, so that their values can only be approximately estimated. This results in some uncertainty in the ratio, B/A, required, and this is consequently reflected in the calculated values for p_m and y_k, which depends on p_m. However, for the friction value selected, $\phi = 32^o$, a lateral earth pressure coefficient K_0, of 0.4*, soil effective (buoyant) unit weight of 0.03461 pci and the pile diameter of 24 inches, the various quantities are calculated for each of the depths of interest according to the RP2A formulas and they are shown in Table 2. In the table, the value of p_k was calculated from y_k using stiffnesses obtained from multiplying 25 pci (k_1) by the depth. It is seen that the uncertainty associated with the ratio B/A is reflected by erratic numbers for y_k, and, consequently, for p_k. Using the values for p and y at the points k, m, and u, the curves at the 8, 25,...,150 inch depths can be calculated and are shown in Figure 7. From the coordinates (y_u,p_u) and (y_m,p_m) the "plastic" slope or modulus can be computed for each depth for comparison with that in Table 1. Since $(y_u - y_m)$ is constant with depth, the slope can be obtained simply, and is shown in the last row of Table 2.

Although somewhat smaller than the initial values in Table 1, it can be observed that the computed values in Table 2 are not altogether inconsistent with them.

---

*The value of $K_0 = 0.4$ was selected because the model pile was pushed into the soil at 1g, and it is not considered that this would generate a high lateral coefficient. Were the pile driven at 100g, a substantially higher value of K_0 would be required.

Table 2

Depth (inch)	8	25	50	75	100	125	150
p_u (lb/in)	66	225	445	653	900	1340	1865
p_m (lb/in)	48	166	333	433	540	755	1050
y_k (in)	0.20	0.23	0.23	0.16	0.11	0.11	0.16
p_k (lb/in)	40	144	288	300	275	344	600
"plastic" slope, psi	36	118	224	440	720	1170	1630

Because of the arbitrary, test-related nature of the constant A, it can be seen that the values of p_u plotted in Figure 7 do not increase smoothly with depth as would be expected. Since p_m depends on A, B and p_u, its values are also somewhat irregular. The parameters p_k and y_k have already been discussed. In consequence the parabolic portions of curves intended to run from (y_k,p_k) to (y_m,p_m) are difficult to plot, and have been omitted.

As a result of the effort to obtain p-y curves, using only the RP2A equations and plots of the parameters A and B, one or two comments are perhaps in order. From a reading of the original paper on the Mustang Island pile tests, it is seen that A was obtained as a correction to the computed value of the ultimate resistance of the soil, p_c. "Values of A were obtained by dividing the observed ultimate soil resistance by the computed ultimate resistance." On the other hand, B was calculated by dividing the measured value of p_m by the calculated p_c. In each case, points representing A and B values at various discrete depths were plotted as functions of dimensionless depth, and smooth curves drawn through them. From these curves, values of A and B must be picked off at various depths

in order to describe a particular test like the present one. It is not surprising that a resultant curve, B/A, required in the analysis, may give uneven results.

If this p-y method is to continue in use, it is suggested that some examination of the functions A, B, and B/A be made, so that they can be appropriately adjusted to give smooth and consistent variations of the derived values of p with depth. Tables of adjusted values to accompany the figures in RP2A would also greatly assist in computations.

However, the p-y method seems to be unduly complicated, considering that the final results desired are usually the load/displacement relation at the top of the pile, and the maximum moment in the pile. The principal aspects of either the load-displacement function or the moment are unlikely to depend strongly on the details of the p-y curve, in particular, on the parabolic portion. In addition, it seems unlikely that, in the normal range of pile loading and response, the flat portion of the p-y curve, beyond y_u = 3D/80, will be reached, except possibly very close to the soil surface.

A simplification of the p-y curve therefore is suggested. It consists of a bilinear p-y function, elastic-plastic, with no ultimate level of plastic resistance. For at least preliminary analyses, the determination of the properties of the bilinear curve can be made as simple as possible, as follows.

(a) Elastic portion: Choose the slope of the straight line (k_1 times depth) equal to the value E of the soil, obtained either from site measurements, or from tables. The value of E corresponds to that of a strain of about 1% and will vary with depth. This selection is arrived at through the results of the Appendix,

where it was found that the plane strain stiffness was approximately equal to E for a range of Poisson's ratios.

(b) End of elastic portion: At any depth, take the termination of the linearly elastic response to occur at a force/unit length in the pile as given by the result in the Appendix where the force F_k at the beginning of plastic behavior is indicated by the equation

$$\frac{\sigma_0' D}{F_k} = \frac{1}{\pi}\left[\frac{1}{\sin^2 \phi} + \frac{1}{3-4\nu}\right]^{\frac{1}{2}} \qquad (A.28)$$

in which σ_0' is the effective lateral stress in the soil ($= K_0\sigma_v'$), D is the pile diameter, ν the Poisson's ratio of the soil and ϕ the angle of friction.* Values of $\sigma_0' a/F_k$, where a is the pile radius, or half that in the above equation, are given in Figure A.10. The displacement, y_k, at the end of elastic straining is given by F_k/E.

(c) Plastic portion: Assume that the slope of the plastic straight line portion of the curve at any depth is one-quarter of the elastic slope at that level, or E/4. The plastic line extends indefinitely.

---

*We have considered only sands here, since the centrifuge tests were conducted in that material. Similar relations can be worked out for clays, and the relevant results are available in the Appendix.

CONCLUSIONS

A method of analysis of data from lateral load tests on piles has been developed. In order to check its validity it has been applied to tests on a model pile imbedded in a Winkler foundation made of rubber blocks of known properties. When the model pile strain gauge readings were analyzed by the proposed method, the load-displacement curves resulting were close to straight lines of slope equal to the stiffness of the rubber blocks, as determined independently.

The method was subsequently applied to the analysis of data from centrifuge tests on laterally-loaded model piles in dry and saturated sands. The force-displacement curves produced ("p-y" curves) were more consistent than those found from previous analysis methods (3), and have been used to develop soil properties as a function of depth along the pile.

These properties have been compared with those found by computation using the API RP2A suggested approach to obtaining p-y curves and a reasonable agreement was found. As a consequence of calculating the p-y curves, some difficulties were found and pointed out. Following this, a simplified technique of deriving p-y curves based on the centrifuge test behavior has been suggested. It will have to be tested, and possibly modified, on the basis of comparisons with other centrifuge tests and, preferably, full-scale experiments.

MODEL PILE-DRIVER TESTS

Several preliminary attempts have been made to construct an apparatus with which model piles can be driven into the soil in the centrifuge while the experimental package is in flight. There are several difficulties in doing this: (a) the model pile-driver impacts should be properly scaled as to energy, from the prototype; (b) the pile-driver should follow the pile-head down; (c) following driving, it should be possible to test-load the pile axially, recording load and displacement to failure. The idea of driving the pile the entire depth of embedment was abandoned at the beginning, because of the problems of supporting the pile until driving commenced, and subsequently removing the support. Consequently, the pile was partially embedded in the soil, and driving attempted for the last inch or two of model pile emplacement. This distance should be sufficient to establish the soil stress state relevant to a driven pile, in terms of its influence on subsequent loading.

At the prototype level, the model approximately represented, at 100g, a pile about 67 ft long, 24 inches in diameter, although the EA of the model pile was too large, and not to scale (it was the pile formerly used for lateral load tests, constructed so that the EI was correct). Such a prototype pile would typically be driven by a pile driver impacting at an energy of several tens of thousands of ft-lb per blow. If the value is taken as 50,000, and the scaling factor for energy in the centrifuge is 100^3 (at 100g) then the model pile driver should have the capability of delivering about 0.6 of an inch-lb per blow. A prototype driver employs a weight of several tons dropping several feet to deliver the blow. At the model scale, the weight would then fall about 0.5 inches and would

have to weigh, therefore, about one pound, at 100g. In consequence, at 1g, the weight employed in the model pile driver would be about 1/100 pound, or 1/6 of an ounce. In practice, it was more convenient to decrease the height of fall somewhat in the model and to use driving weights in the range of 1/2 to 1 ounce. Thus, the steel driving weight was required to have a diameter of 0.2 to 0.3 inches and a length of about 1 or 2 inches. These dimensions scale (1/100) from those of the prototype also.

A prototype pile-driver delivers about one blow a second to a pile; if this were to be modeled with centrifuge dynamic scaling, the model driver would have to be operated at a rate of 100 blows per second. However, since it was intended to try to record the pile behavior for each blow, it was decided not to provide this rate in the model. In addition, although there is probably some dynamic, repetitive impact effect in prototype driving, the pile vibrations are probably stilled after one blow, before the next blow is struck. If this is indeed the case, the dynamic effects of successive blows are unrelated and the phenomena associated with one blow are adequate for study. That is not to say that there are no transient occurrences during the impacts; pore pressures are certainly developed in saturated soils, and in the prototype, do not have time to dissipate much between impacts when the soils are fine-grained. In the model, careful attention will have to be paid to such effects in certain soils, since the time scaling for pore-water diffusion effects goes as 100^2 (100g tests). It is possible that, for example, in the saturated fine "Nevada" test sand, little or no porewater dissipation would take place between one-a-second prototype impacts, whereas, in the model, significant dissipation, occurring 100^2 faster, could develop in the same soil between

blows only 100 times more rapid. Since the preliminary tests were performed in dry sand, this problem was avoided.

The most difficult requirement to fulfill was that of following the pile down, while still providing a means of carrying out a static pile test at the end of driving. Since the pile was intended to move one or two inches, and then to be subjected to a static test in which it was necessary to resolve displacements to within a range of 10^{-4} to 10^{-3} inches, two different displacement-sensing mechanisms were required. The initial design involved using a solenoid as the pile driver; switching of the current caused lifting and release of the iron core. The rate could be varied, but could not be raised to the 100 Hertz level required, because at 100g, the solenoid core was not being lifted far enough. In effect, it merely twitched. The reason was the small size of the coil employed. A thicker winding would have generated more force, but would also have required heavier supports. The poor performance of the solenoid driver at high g-levels led to the abandonment of the device.

A second device was constructed, which was operated by compressed air through a rotating union on the centrifuge to lift and drop a weight via a pneumatic cylinder. This was in concept similar to the full-scale machine which uses steam. Some success was achieved in driving the model pile with this apparatus. A section of the traces obtained on a miniature accelerometer attached to the pile top and from the strain gauges is shown in Figure 8. It is seen that peak accelerations of about 210g were obtained.

The arrangement made for following the pile, and loading it statically after driving is illustrated in Figure 9. What it consists of is a counter-weight which almost balances the weight of the pile-driver during driving, so that the driver rests lightly on the pile. When the pile is

fully driven, a collar at its top comes in contact with a sensitive strain-gauged cantilever beam system used for measuring the small displacments of a load test. Underneath the counterweight is mounted an hydraulic cylinder, whose pistion when actuated, moves upward and takes the weight of the counterbalance. Thus the total weight of the driver effectively is brought to bear on the pile. Since it can be weighted additionally, a fairly substantial load can be generated on the pile while the displacements are recorded. Load is registered through a load cell installed serially in the system.

The principal outcome of these tests was to establish the requirements for an effective pile driving and loading system. At the time of writing this report, a modified driving and loading system is being designed. Further and more detailed tests will be performed when it is complete.

REFERENCES

1. American Petroleum Institute RP2A, "Planning, Designing and Constructing Fixed Offshore Platforms," 10th Edition, March 1979.

2. Reese, L.C., Cos, W.R., and F.D. Koop, "Analysis of Laterally Loaded Piles in Sand," Paper OTC 2080, Proc. 6th American Offshore Technology Conference, Houston, May, 1974.

3. Scott, R.F., "Cyclic Lateral Loading of Piles; Analysis of Centrifuge Tests," Report through May 31, 1979 on Research Program for API OSAPR Project 13, California Institute of Technology, June 4, 1979.

ACKNOWLEDGMENTS

The tests described herein were performed by John Lee and the author. John Christenson participated in some of the work. Computer programming asssistance was supplied by Albert Chang. Sharon Vedrode typed the report.

FIGURE CAPTIONS

Figure Number	Caption
1	Model pile and loading wire in rubber block Winkler foundation: (a) General view; (b) Close-up.
2	Spline fit to rubber Winkler tests: (a) Moment; (b) Shear; (c) Pressure; (d) Displacement; (e) Slope; (f) Pressure versus displacement.
3	Combination polynomial/spline fit to rubber Winkler tests: (a) Moment; (b) Pressure; (c) Displacement; (d) Pressure versus displacement for low clamping pressure; (e) Pressure versus displacement for high clamping pressure.
4	Polynomial/spline fit to centrifuge tests in dry sand: pressure versus displacement: (a) first cycle of load/unload; (b) second cycle.
5	Polynomial/spline fit to centrifuge tests in saturated sand: pressure versus displacement: (a) first cycle of load/unload, (with overlay of Figure 7); (b) second cycle.
6	Elastic and plastic coefficients versus vertical effective stress in soil. Circles and triangles represent data on elastic coefficients from dry and saturated sand tests respectively. For these the scale at the top of the figure applies. Flagged circles and triangles indicate the plastic coefficients, for which the scale at bottom right should be employed. The open symbols are points for the earlier analysis (3); filled symbols from the present work.
7	Pressure-displacement ("p-y") curves calculated from RP2A.
8	Traces of accelerometer and strain gauges during pile-driving.
9	Pile-driver and pile loading arrangement: (a) Pile driver; (b) Pile, pile-driver and pile-loading arrangement.

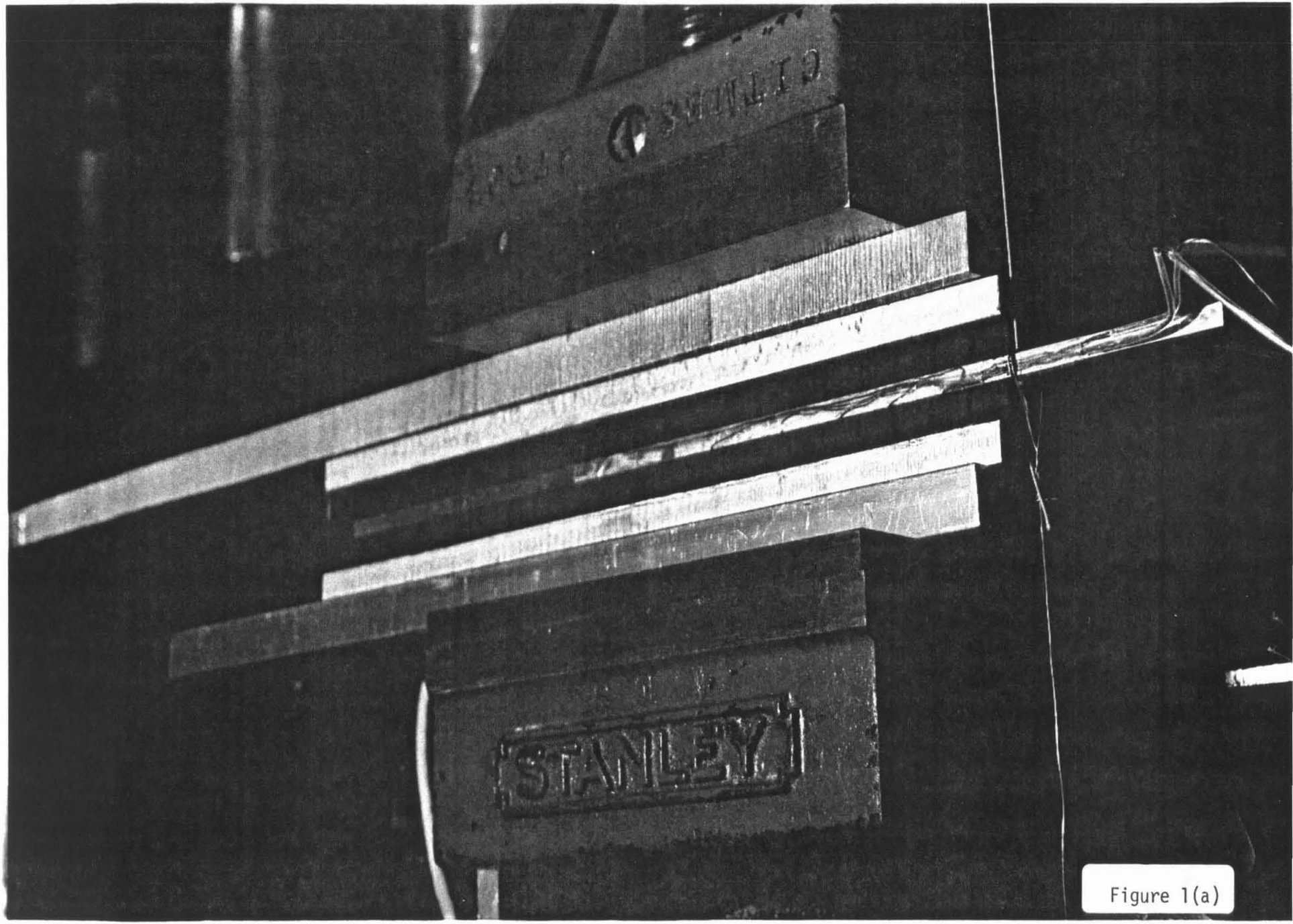

Figure 1(a)

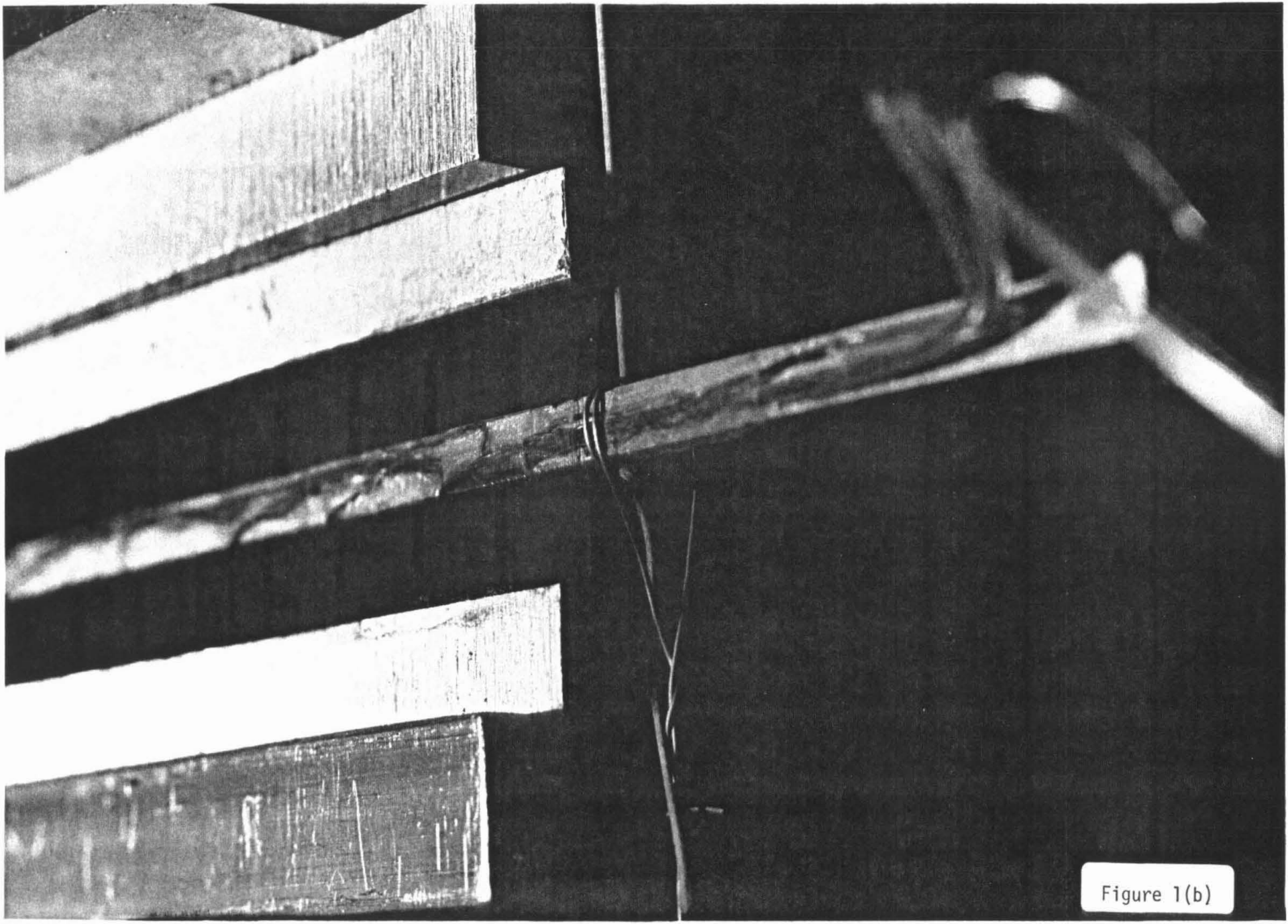

Figure 1(b)

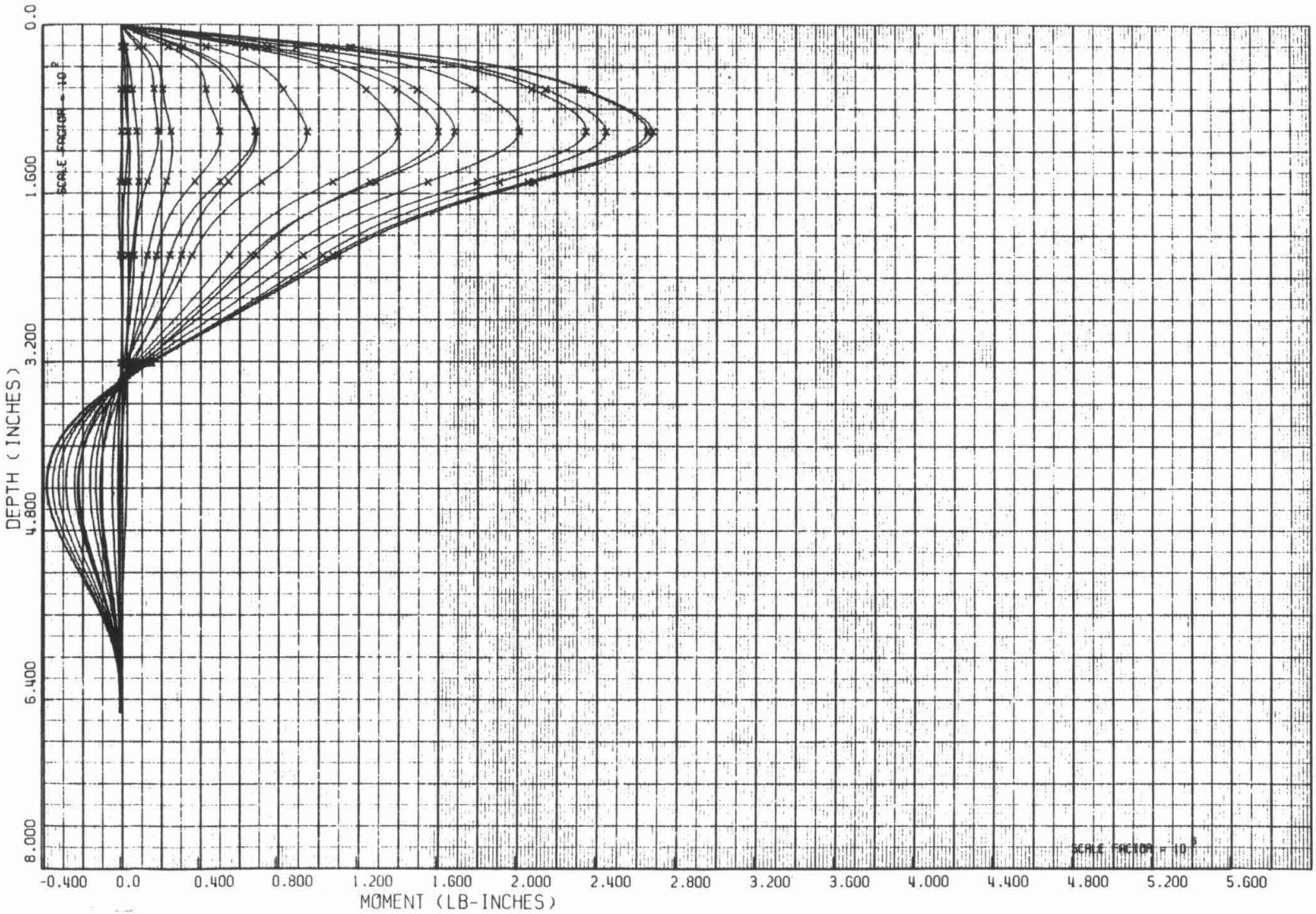
0.0
1.600
3.200
4.800
6.400
8.000
DEPTH (INCHES)
SCALE FACTOR = 10^2
SCALE FACTOR = 10^5
-0.400
0.0
0.400
0.800
1.200
1.600
2.000
2.400
2.800
3.200
3.600
4.000
4.400
4.800
5.200
5.600
MOMENT (LB-INCHES)

Figure 2(a)

DEPTH (INCHES)
0.0
1.600
3.200
4.800
6.400
8.000
SCALE FACTOR = 10²
0.400
0.0
-0.400
-0.800
-1.200
-1.600
DEPTH (INCHES)
0.0
1.600
3.200
4.800
6.400
8.000
SCALE FACTOR = 10²
-0.800
-0.400
0.0
0.400
0.800
1.200

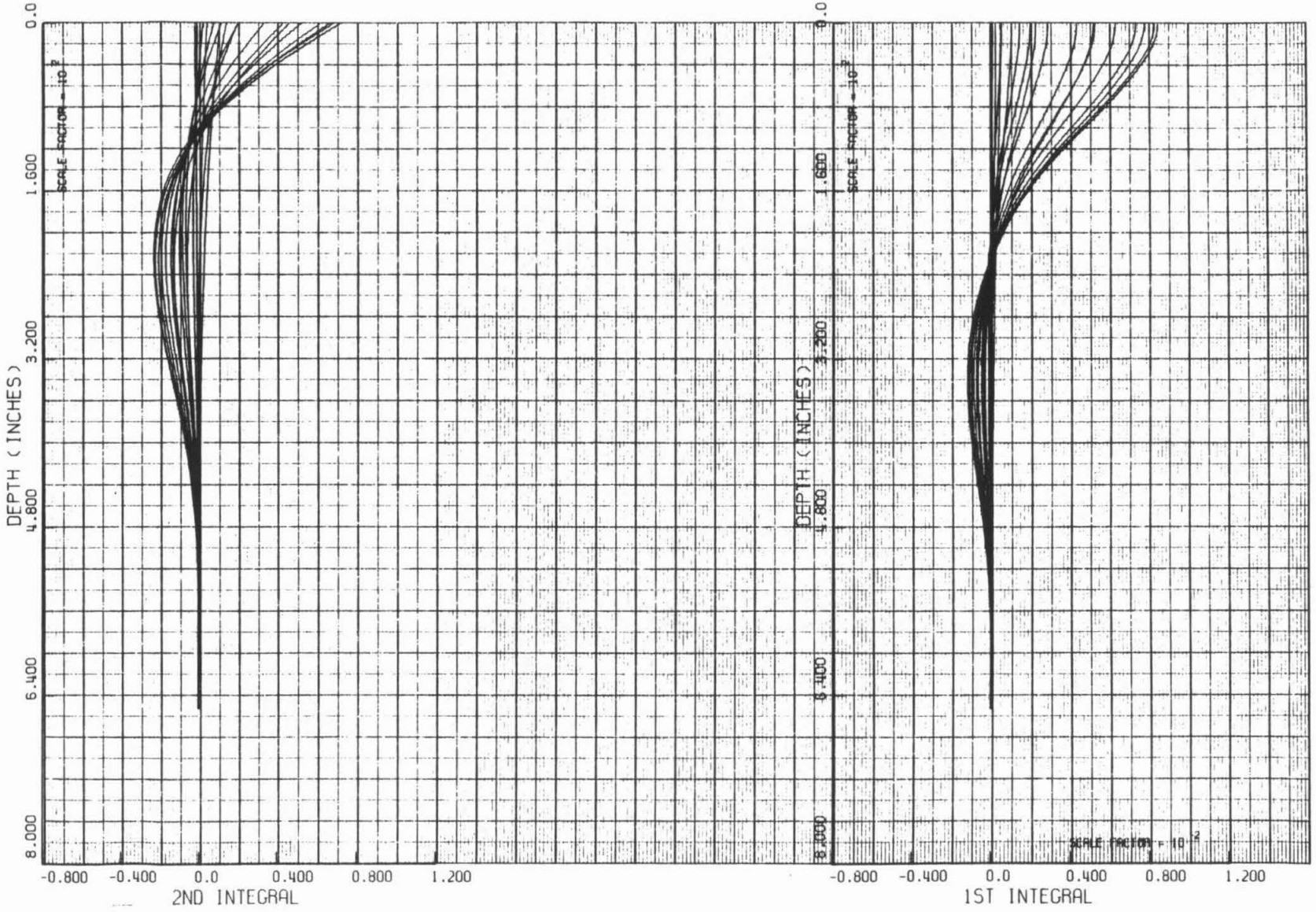

Figure 2(d)

Figure 2(e)

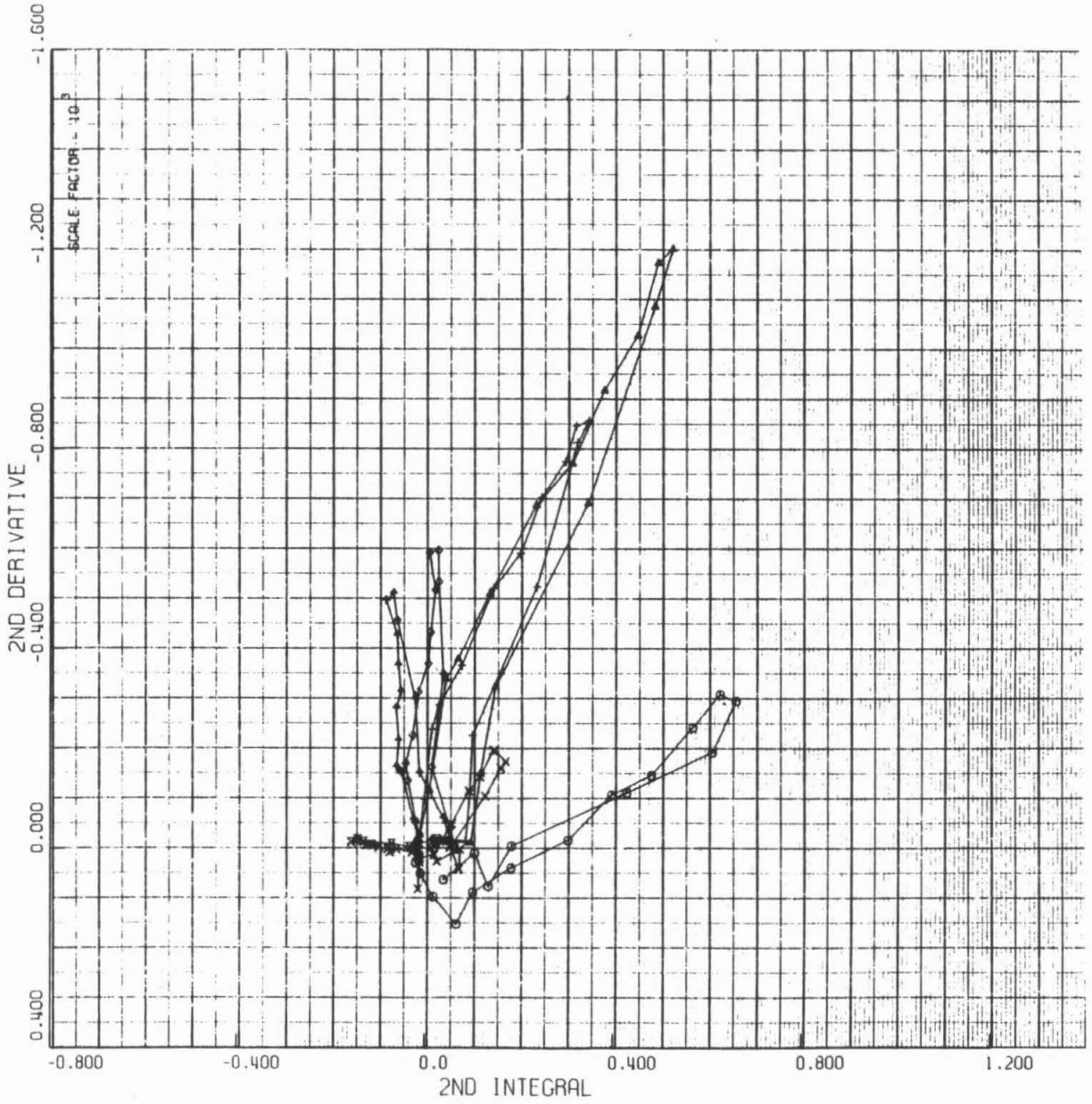
SCALE FACTOR = 10^3
2ND DERIVATIVE
-1.600
-1.200
-0.800
-0.400
0.000
0.400
-0.800
-0.400
0.0
0.400
0.800
1.200
2ND INTEGRAL

Figure 2(f)

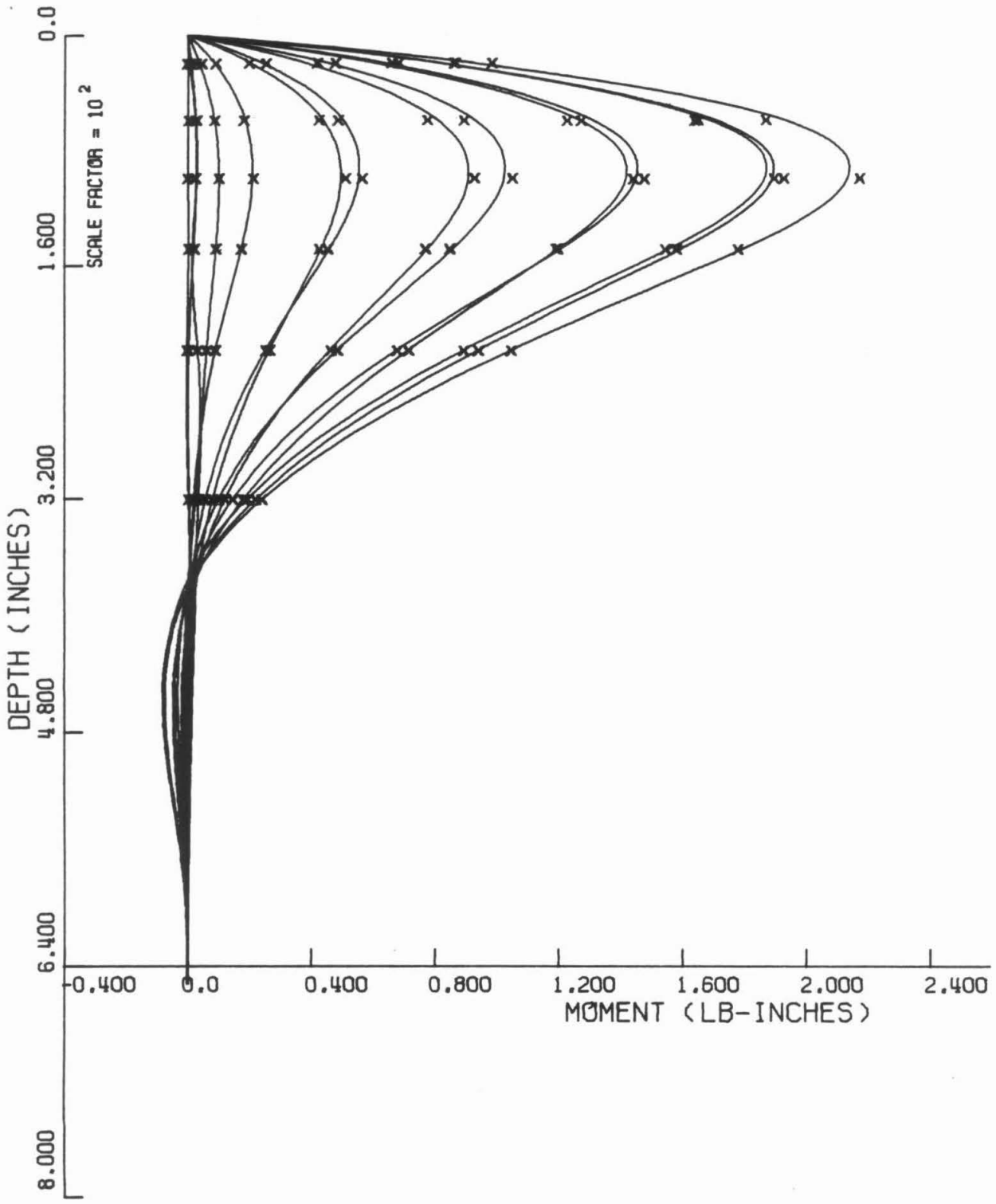
SCALE FACTOR = 10^2
DEPTH (INCHES)
0.0
1.600
3.200
4.800
6.400
8.000
-0.400
0.0
0.400
0.800
1.200
1.600
2.000
2.400
MOMENT (LB-INCHES)

Figure 3(a)

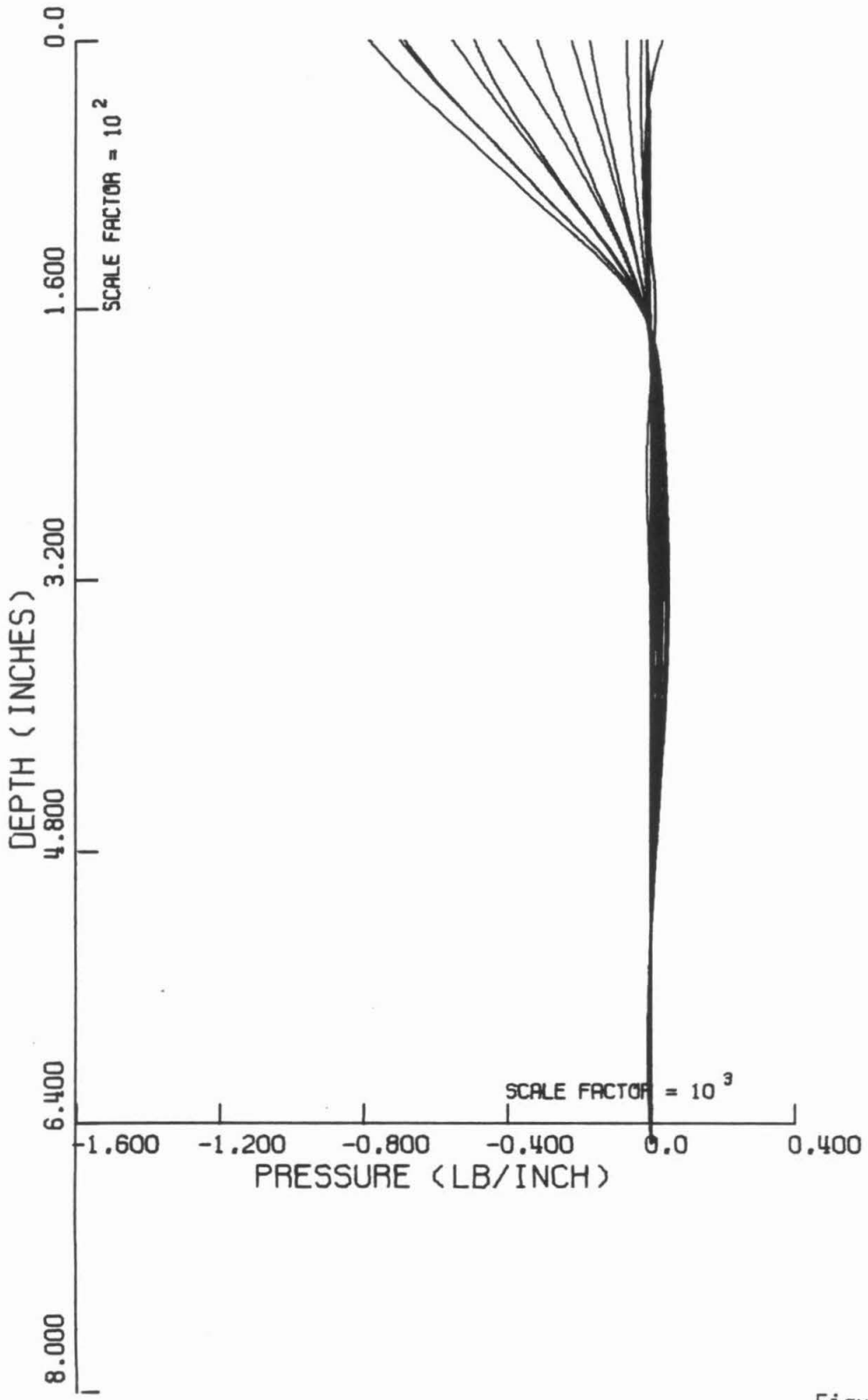
0.0
1.600
3.200
4.800
6.400
8.000
DEPTH (INCHES)
SCALE FACTOR = 10 2
SCALE FACTOR = 10 3
-1.600
-1.200
-0.800
-0.400
0.0
0.400
PRESSURE (LB/INCH)

Figure 3(b)

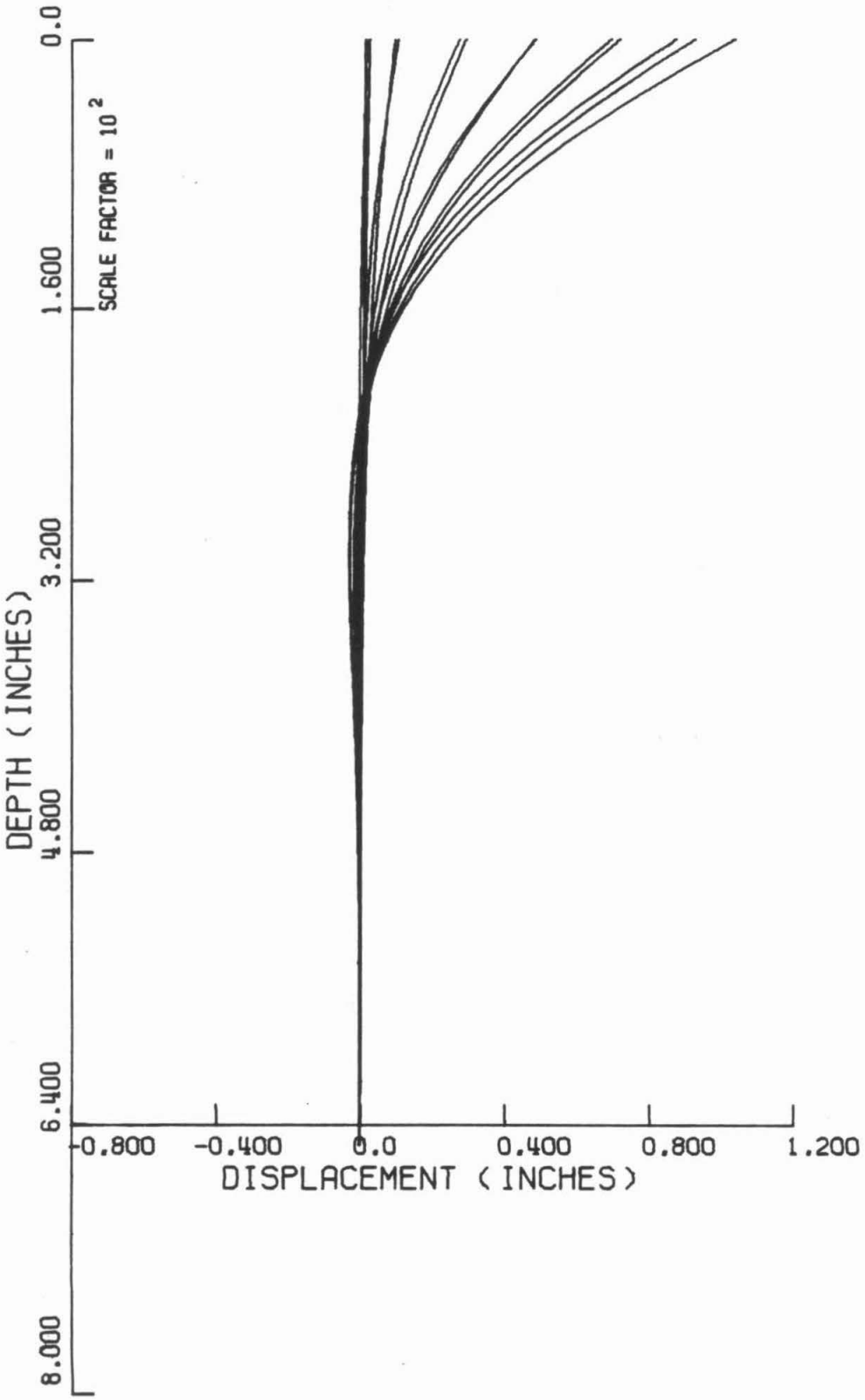
0.0
1.600
3.200
4.800
6.400
8.000
DEPTH (INCHES)
SCALE FACTOR = 10^2
-0.800
-0.400
0.0
0.400
0.800
1.200
DISPLACEMENT (INCHES)

Figure 3(c)

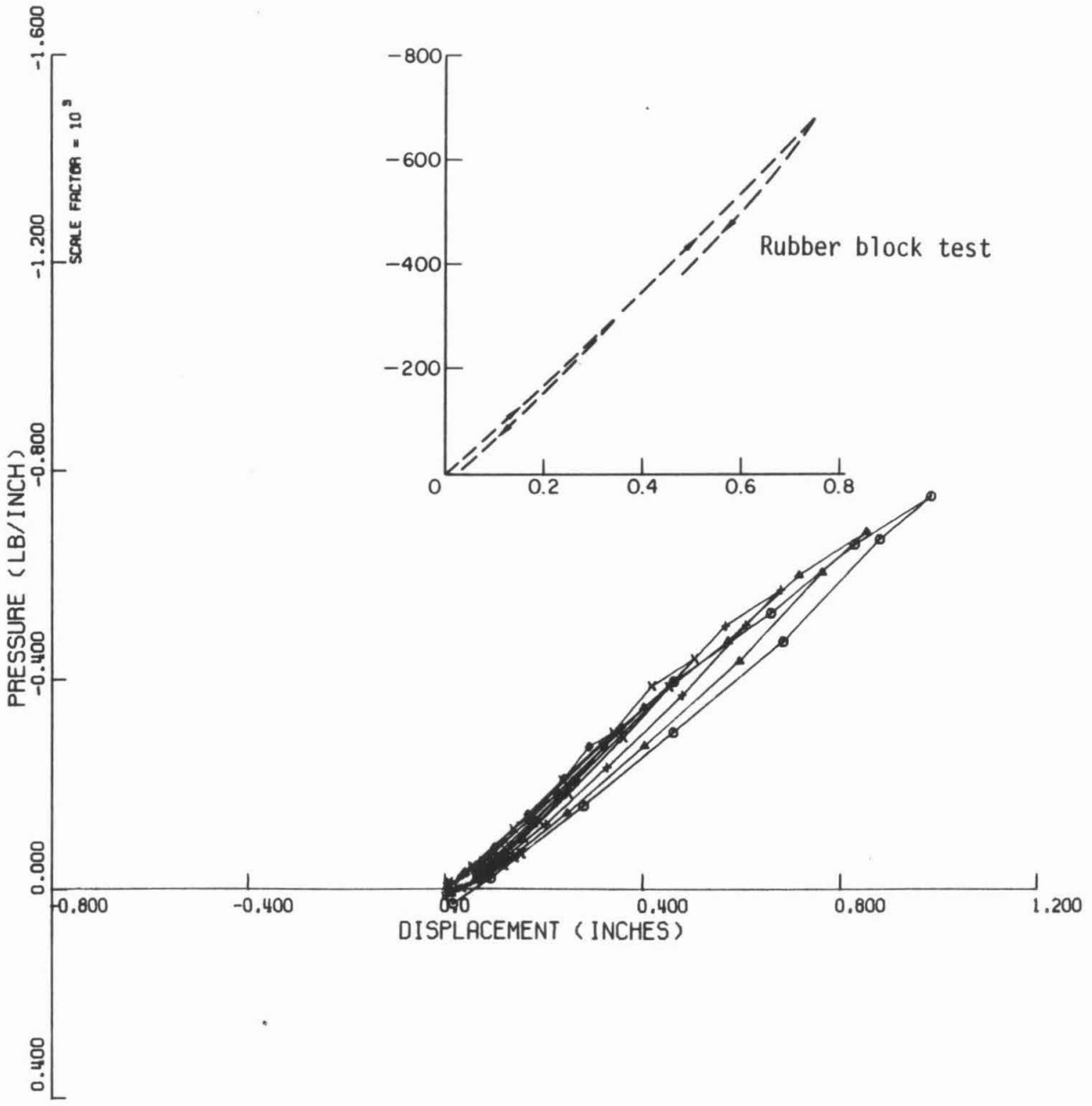
-1.600
-1.200
-0.800
-0.400
0.000
0.400
SCALE FACTOR = 10³
PRESSURE (LB/INCH)
-0.800
-0.400
0.400
0.800
1.200
DISPLACEMENT (INCHES)
-800
-600
-400
-200
0
0.2
0.4
0.6
0.8
Rubber block test

Figure 3(d)

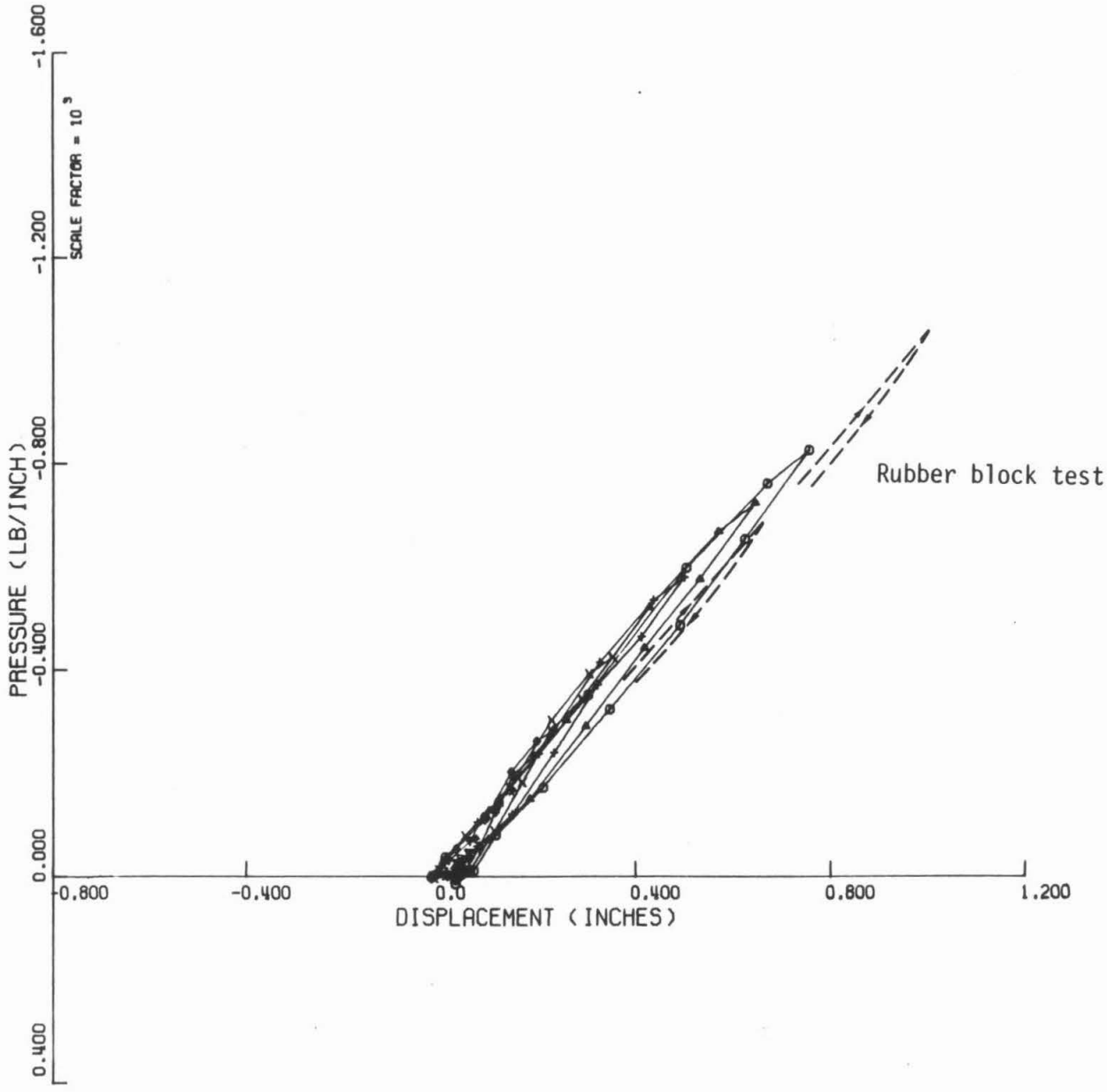
-1.600
-1.200
-0.800
-0.400
0.000
0.400
SCALE FACTOR = 10³
PRESSURE (LB/INCH)
-0.800
-0.400
0.0
0.400
0.800
1.200
DISPLACEMENT (INCHES)
Rubber block test

Figure 3(e)

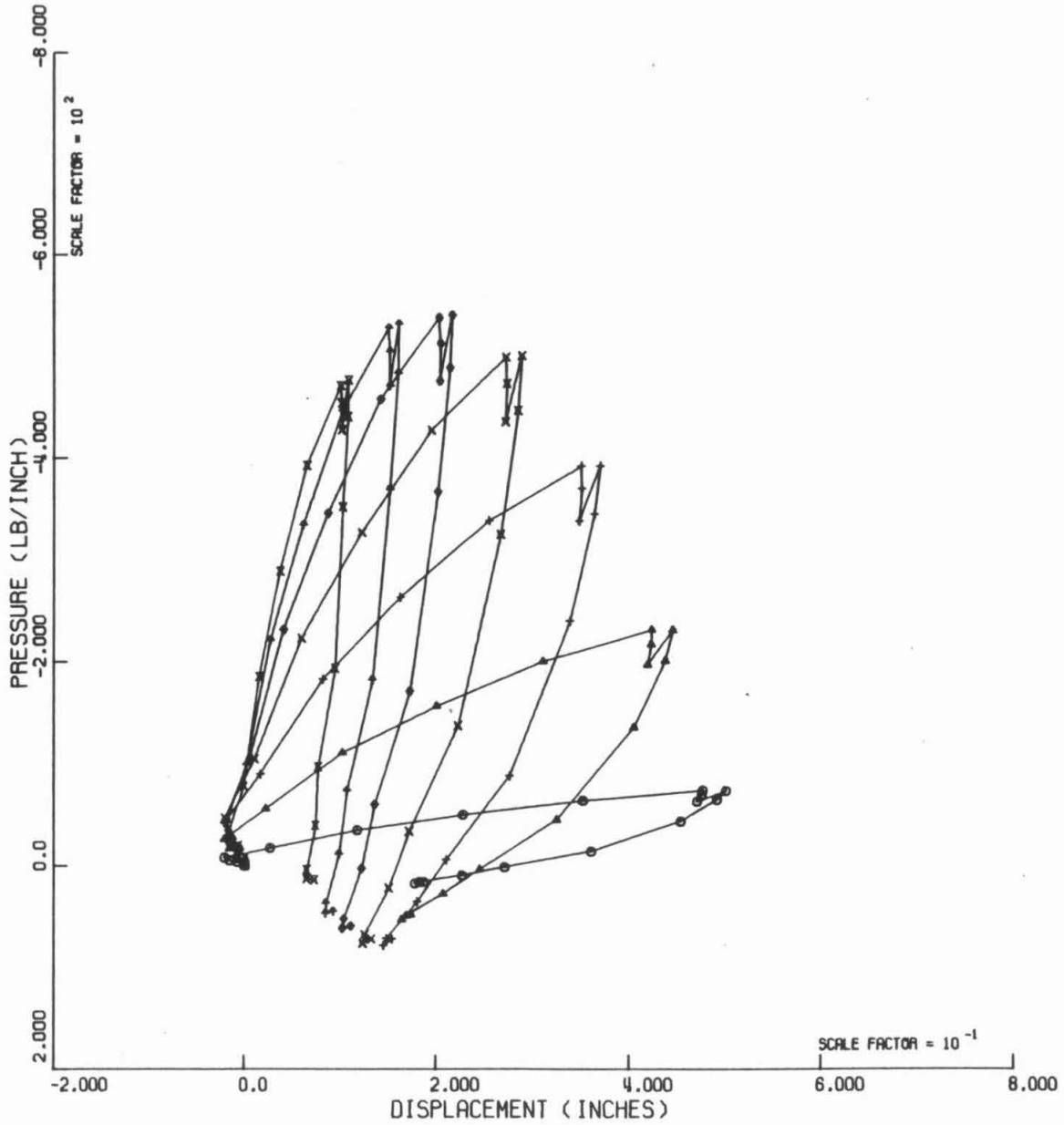
-8.000
-6.000
-4.000
-2.000
0.0
2.000
SCALE FACTOR = 10^2
PRESSURE (LB/INCH)
SCALE FACTOR = 10^{-1}
-2.000
0.0
2.000
4.000
6.000
8.000
DISPLACEMENT (INCHES)

Figure 4(a)

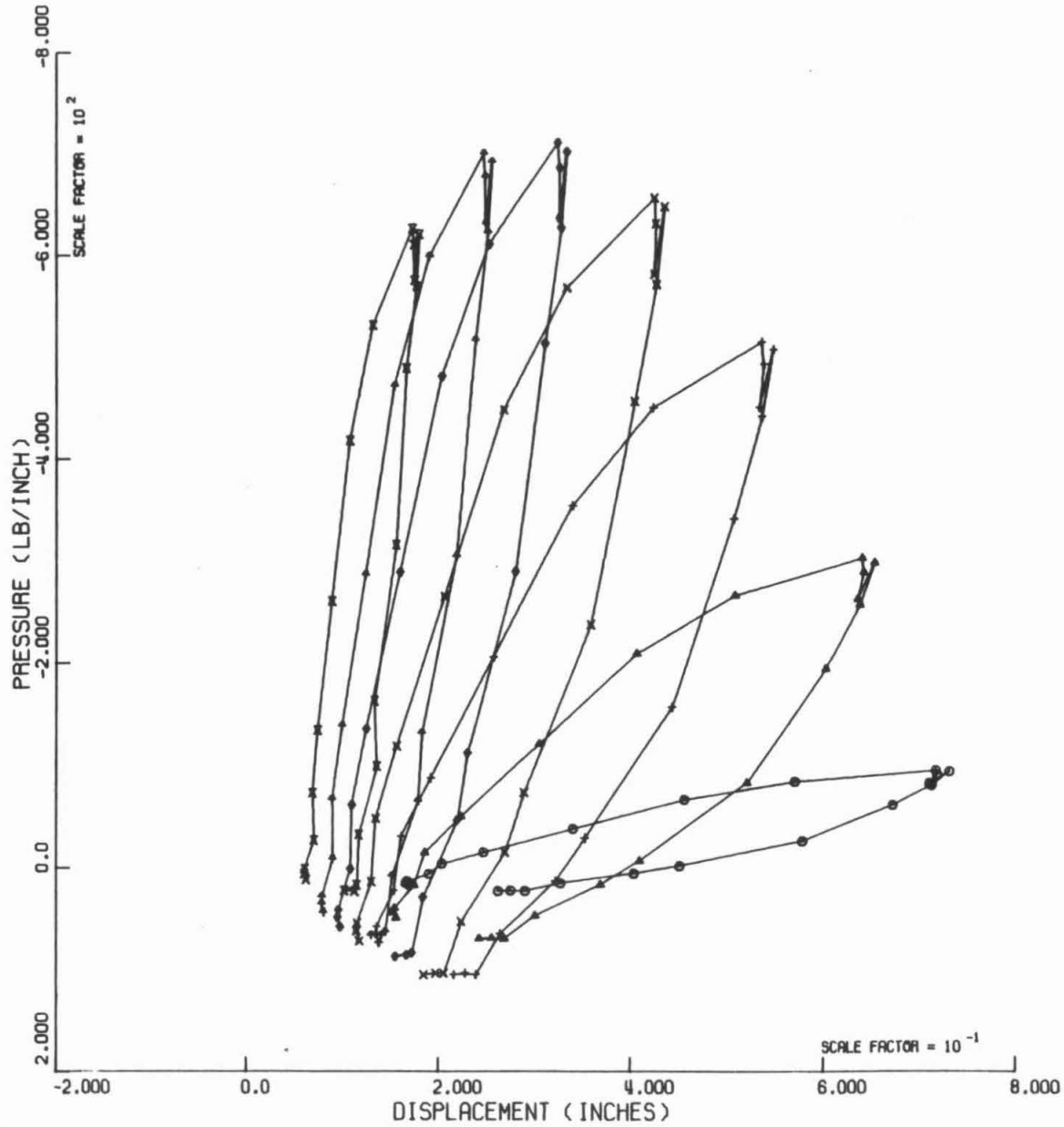
-8.000
-6.000
-4.000
-2.000
0.0
2.000
SCALE FACTOR = 10^2
PRESSURE (LB/INCH)
SCALE FACTOR = 10^{-1}
-2.000
0.0
2.000
4.000
6.000
8.000
DISPLACEMENT (INCHES)

Figure 4(b)

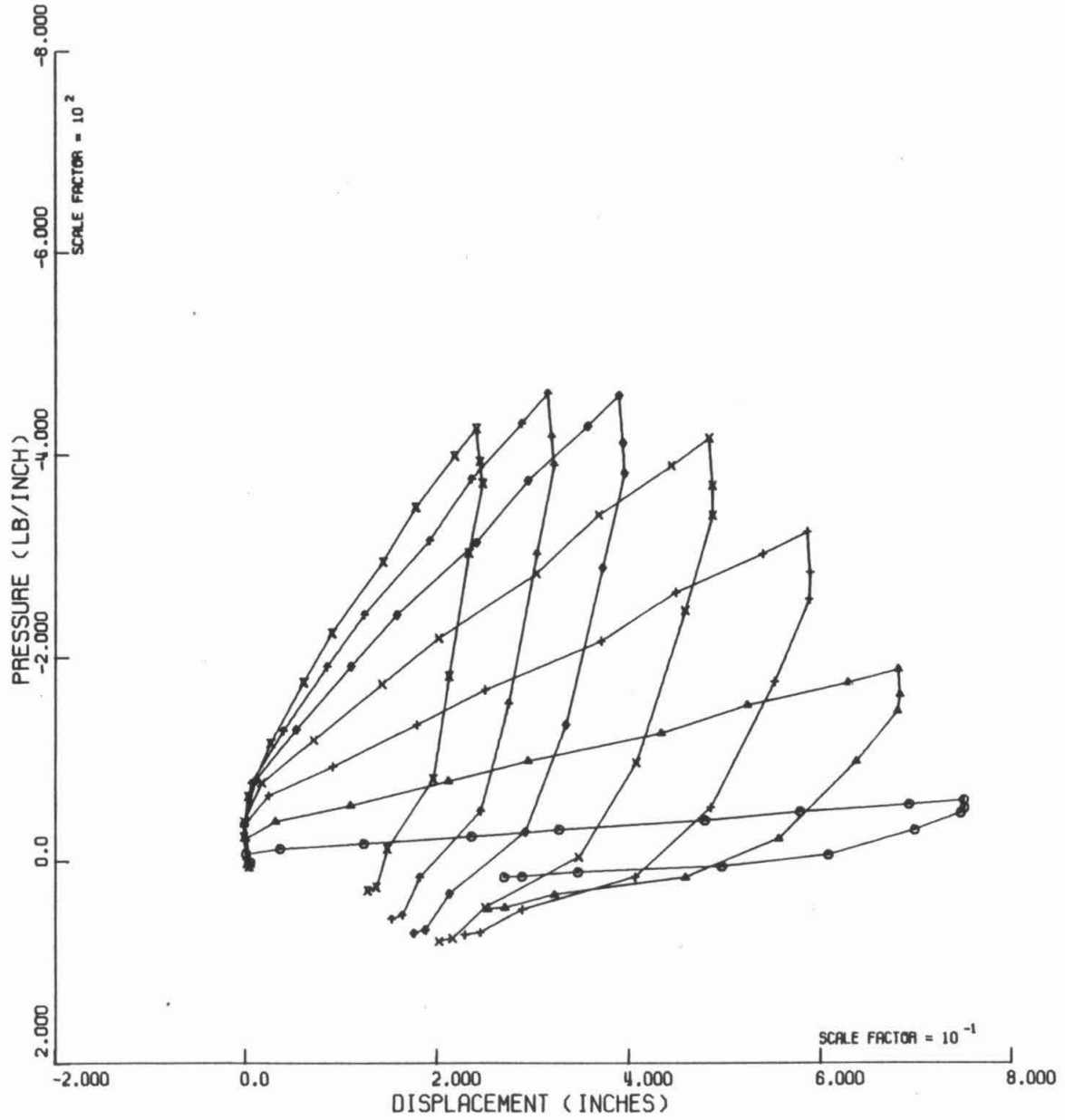
-8.000
-6.000
-4.000
-2.000
0.0
2.000
SCALE FACTOR = 10^2
PRESSURE (LB/INCH)
SCALE FACTOR = 10^{-1}
-2.000
0.0
2.000
4.000
6.000
8.000
DISPLACEMENT (INCHES)

Figure 5(a)

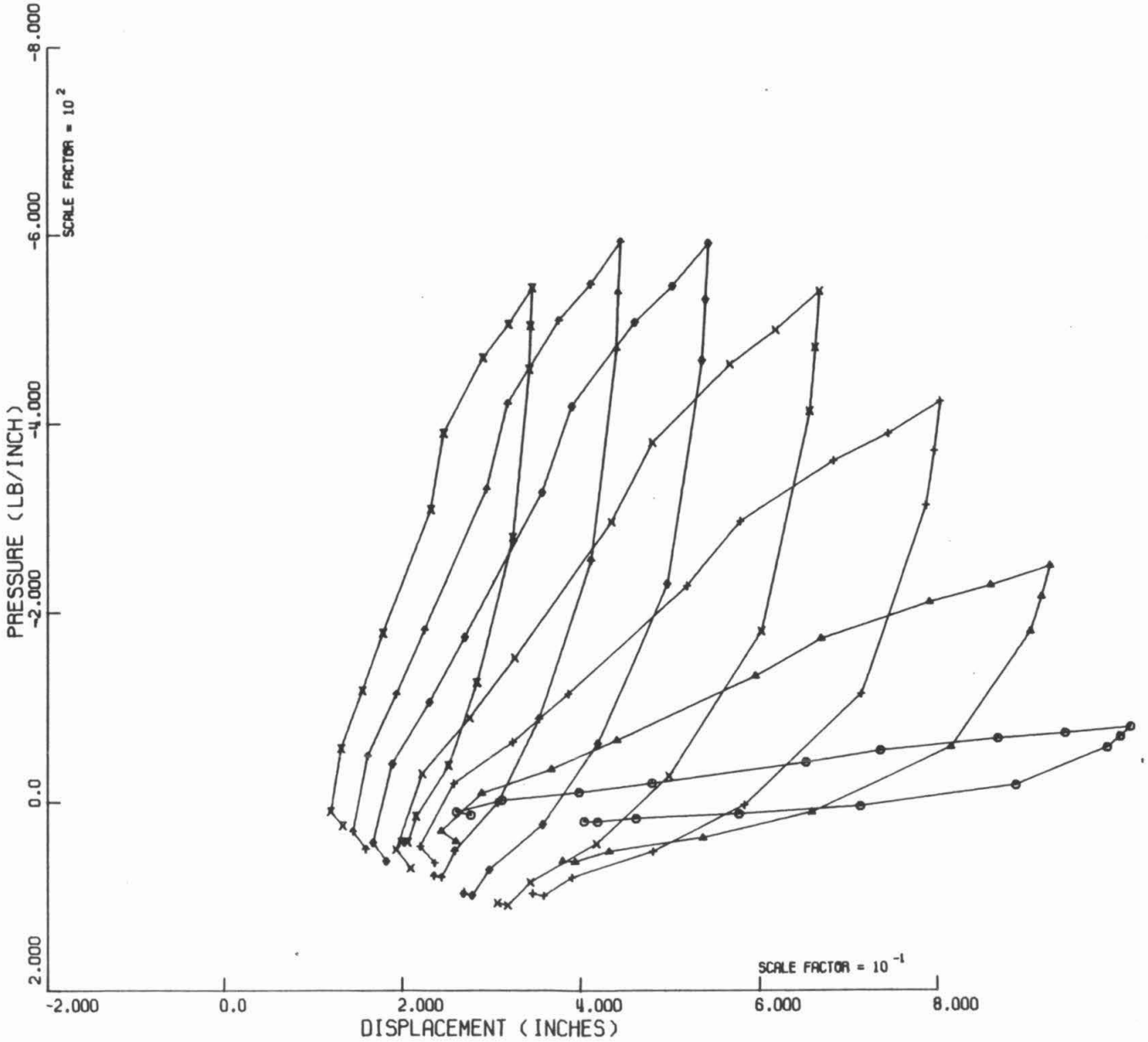
-8.000
-6.000
-4.000
-2.000
0.0
2.000
SCALE FACTOR = 10^2
PRESSURE (LB/INCH)
SCALE FACTOR = 10^{-1}
-2.000
0.0
2.000
4.000
6.000
8.000
DISPLACEMENT (INCHES)

Figure 5(b)

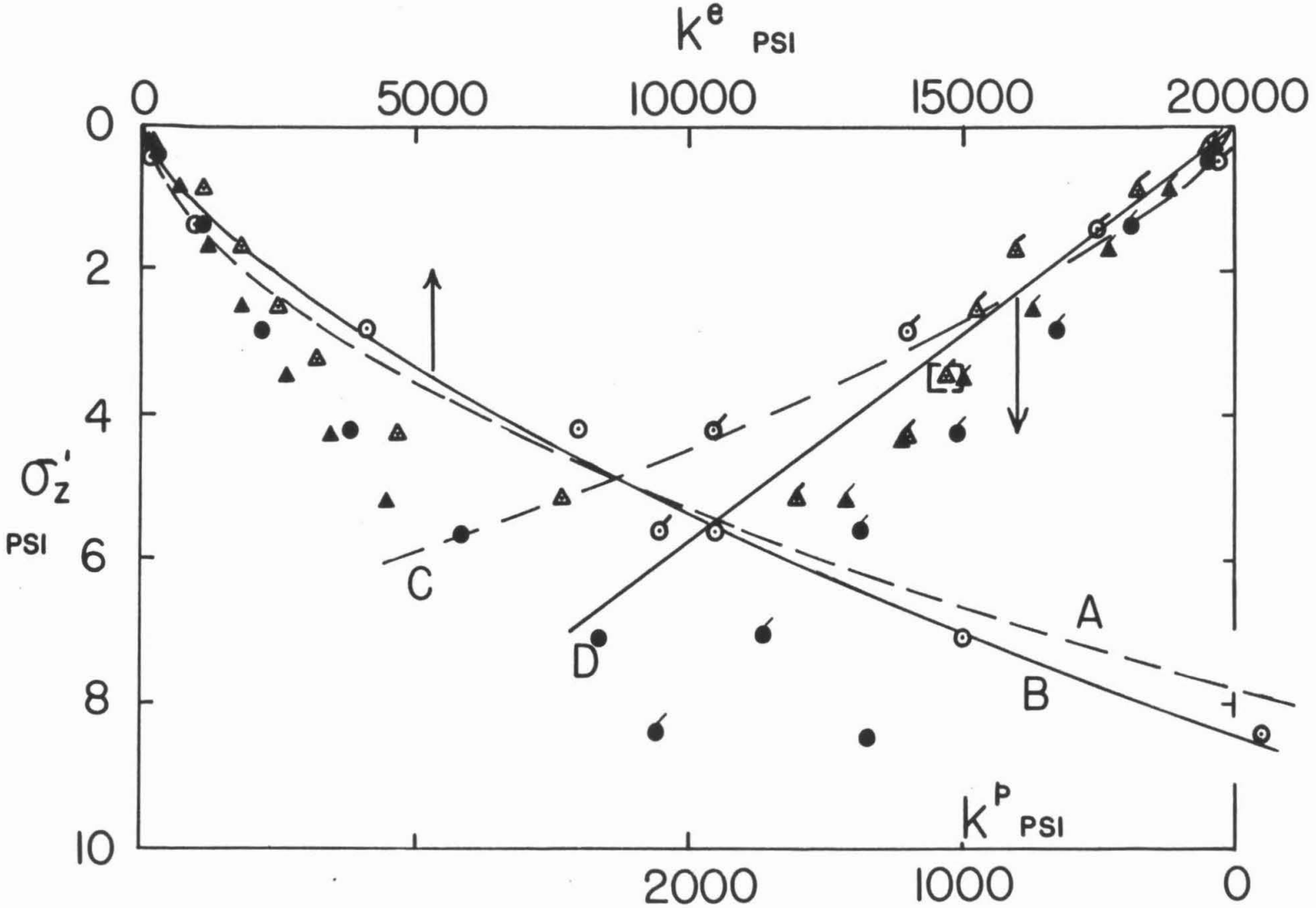
k^e PSI
0
5000
10000
15000
20000
0
2
4
6
8
10
σ_z'
PSI
A
B
C
D
k^p PSI
2000
1000
0

Figure 6

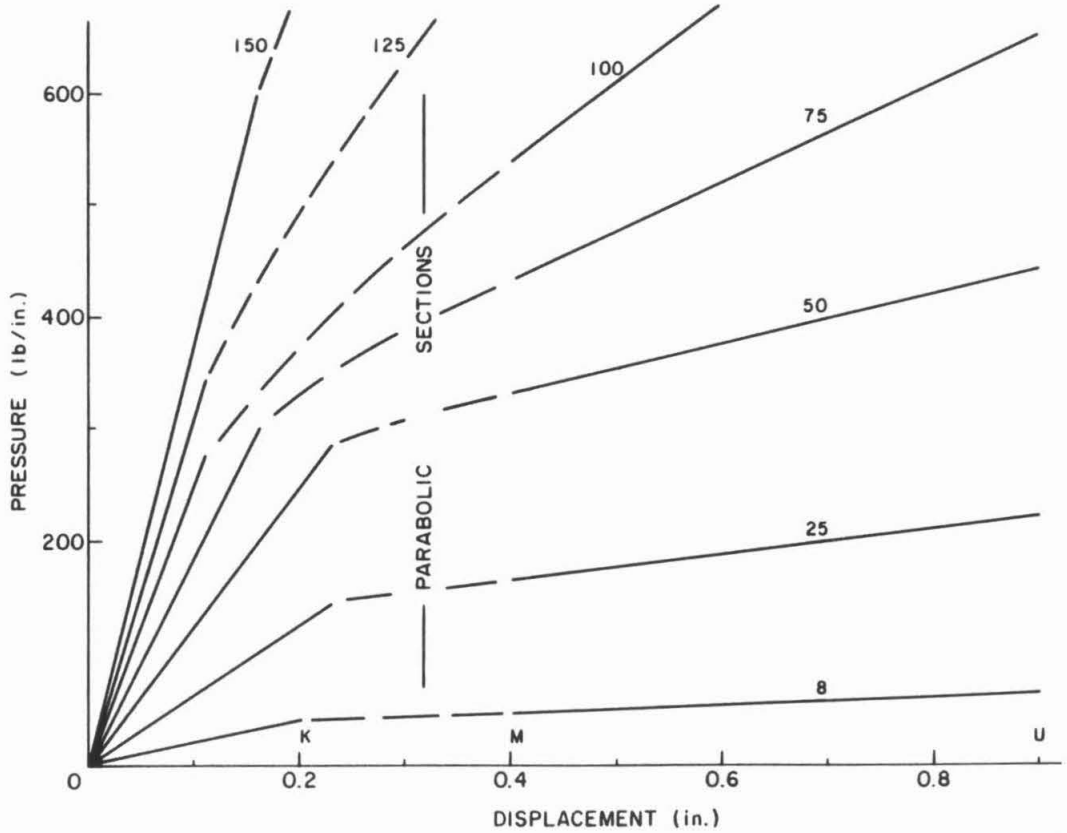
150
125
100
75
50
25
8
600
400
200
0
PRESSURE (lb/in.)
SECTIONS
PARABOLIC
K
M
U
0.2
0.4
0.6
0.8
DISPLACEMENT (in.)

Figure 7

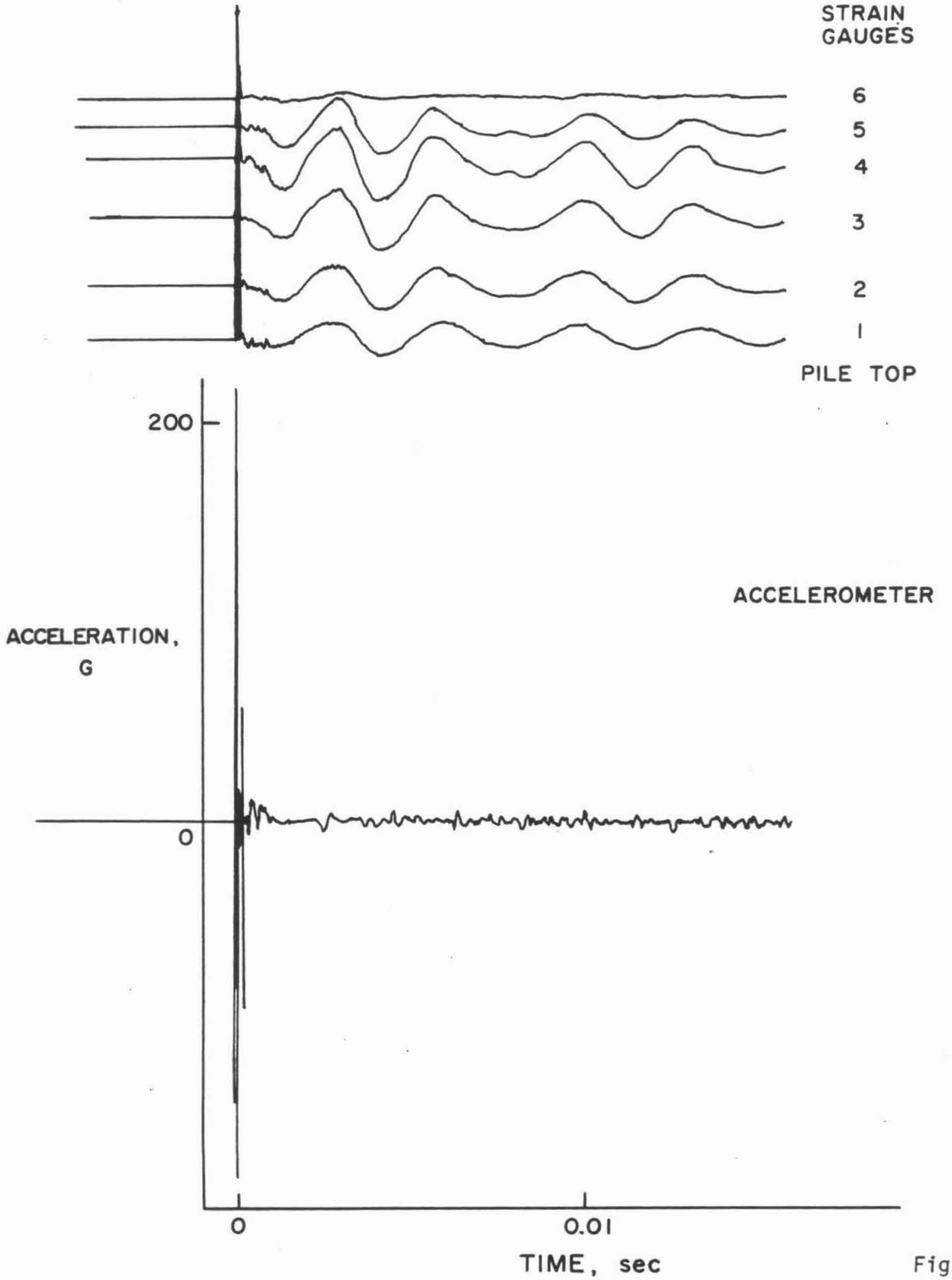
STRAIN GAUGES
6
5
4
3
2
1
PILE TOP
200
ACCELERATION, G
ACCELEROMETER
0
0
0.01
TIME, sec

Figure 8

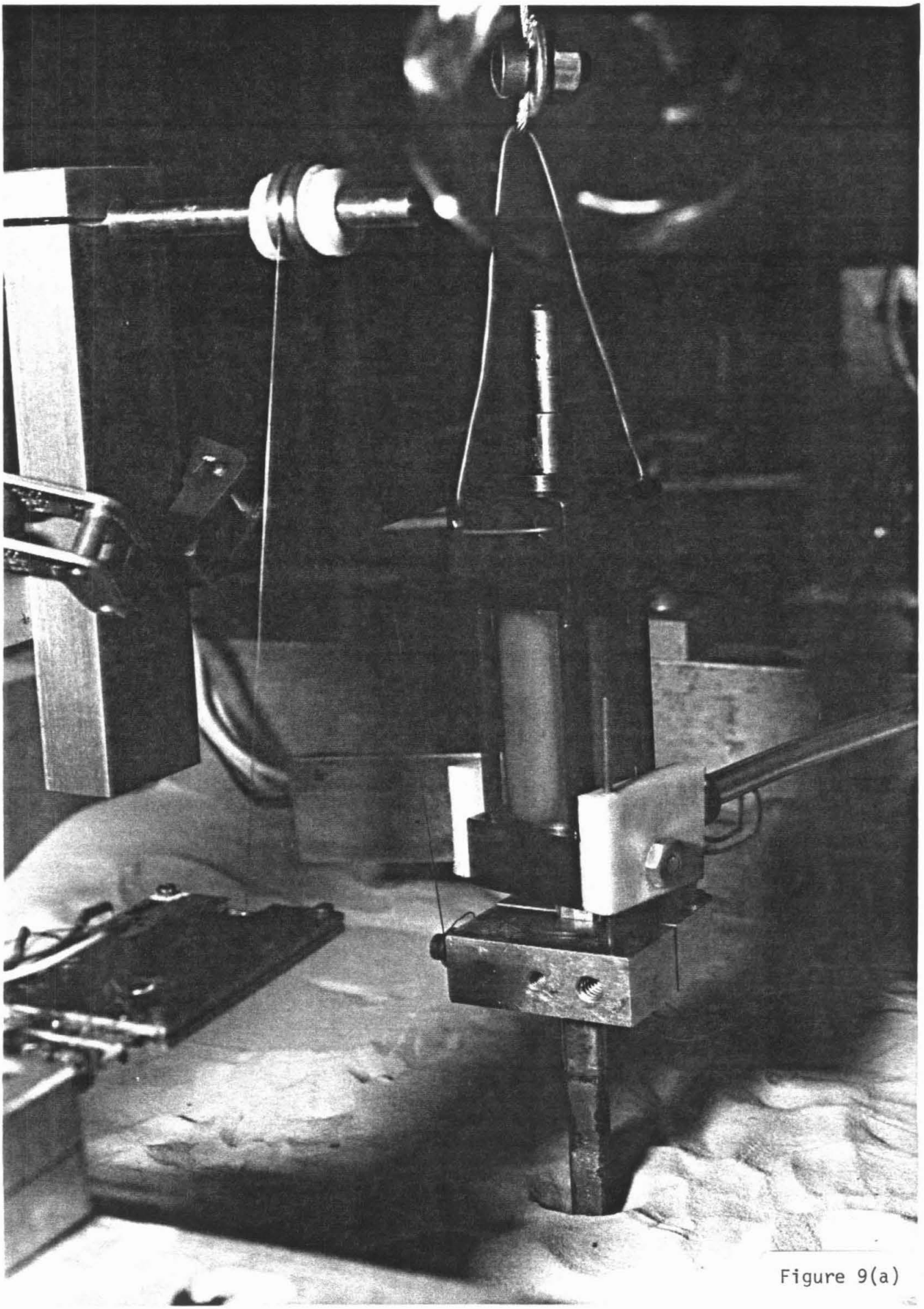

Figure 9(a)

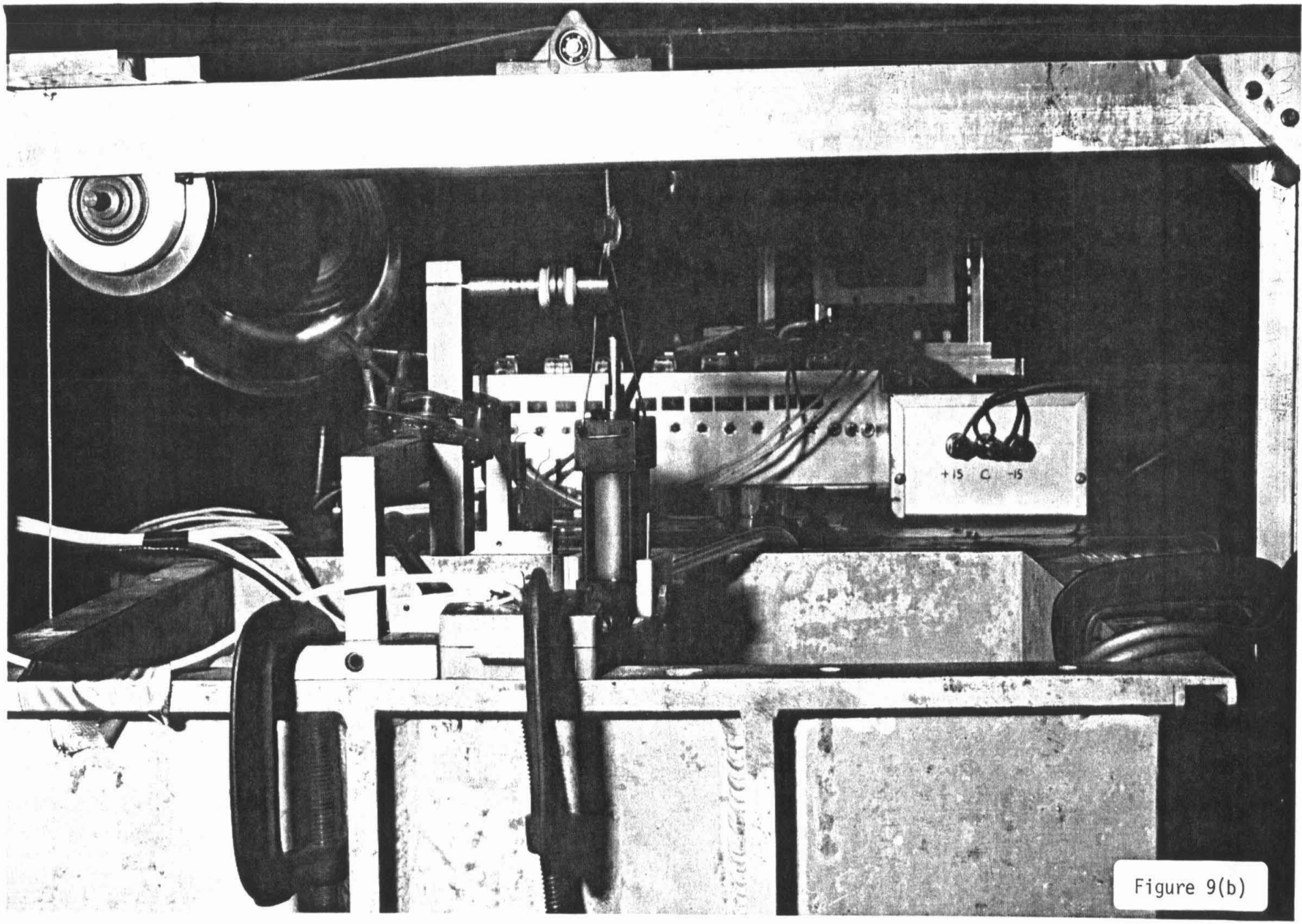

Figure 9(b)

APPENDIX

PLANE STRAIN SOLUTION OF A RIGID CYLINDER MOVING LATERALLY IN AN ELASTIC MEDIUM

Jean-Pierre Bardet*

* Graduate Research Assistant, Division of Engineering and Applied Science, California Institute of Technology, Pasadena, California

PLANE STRAIN SOLUTION OF A RIGID CYLINDER MOVING LATERALLY IN AN ELASTIC MEDIUM

J-P. Bardet

SUMMARY

The plane strain problem of a rigid cylinder moving laterally in an elastic annulus has been solved analytically by Airy stress functions. Displacement on the inner and outer boundaries of the elastic medium are the prescribed boundary conditions. The distribution of radial, tangential, shear and deviatoric stresses in the elastic region is presented. The relation of the lateral displacement of the cylinder to the force acting on it is given. The influence of the size of the elastic region on this relation is studied, its domain of validity is investigated by looking for the onset of plasticity for cohesive and cohesionless materials.

I. INTRODUCTION

When a pile moves in a soil under lateral loading, stresses are developed on its surface and in the soil. In order better to understand the stress distribution around a cylindrical pile, and consequently the soil-pile interaction, a preliminary study of a linearly elastic solution was carried out. In a previous analysis (ref.2), Coker and Filon assumed a given stress boundary condition on the basis of a photoelastic experiment. However their results cannot be applied for our purpose since the rigid disc in their experiment appears to have separated from the embedding material.

In 1977, F.Baguelin et al (ref.1) examined the lateral reaction mechanism of a pile. Starting with the elastic solution, they studied the soil disturbance effect around the pile, and generated a complete displacement load curve including yielding of the soil. However their analysis does not take into account the influence of the size of the elastic domain on the pile

lateral stiffness, and can only be applied to a cohesive material.

The present analysis, which was performed before the Baguelin paper was found, determines a linear relation between the applied load on the rigid cylinder and its displacement for varying size of the elastic medium and its domain of validity for different material. The force-displacement relation can be used to give a winkler reaction modulus.

This approach is reminiscent of the work of Gibson (ref.3) and others who have examined the problem of a radially expanding cylinder.

II. STATEMENT OF PROBLEM, BOUNDARY CONDITIONS

Let us consider a rigid two-dimensional cylinder of radius a, embedded in an elastic cylinder of radius b. The problem is thus plane strain, where E and ν are respectively the Young's modulus and the Poisson's ratio of the elastic domain. No body force exists.

The rigid cylinder (Fig. 1) is moved a distance δ in the x direction, while the outer boundary is fixed. We call the inner boundary Γ_1, the outer boundary Γ_2 and define a point's position by its polar coordinates r,θ. Its displacement is defined by its radial and tangential coordinates u_r and u_θ.

The displacement boundary conditions are given in relation (1) and (2)

$$\text{on } \Gamma_1 \quad r = a \quad u_r = \delta.\cos\theta \tag{1a}$$

$$u_\theta = \delta.\sin\theta \tag{1b}$$

$$\text{on } \Gamma_2 \quad r = b \quad u_r = 0 \tag{2a}$$

$$u_\theta = 0 \tag{2b}$$

According to symmetry about the x axis, the radial and tangential displacements, u_r and u_θ, at any point of the elastic medium satisfy relation (3)

$$u_r(r,\theta) = u_r(r,-\theta) \tag{3a}$$

$$u_\theta(r,\theta) = -u_\theta(r,-\theta) \tag{3b}$$

III. ANALYTICAL SOLUTION WITH AIRY STRESS FUNCTION

A general stress function Φ in polar coordinates (ref.5) is expressed as follows:

$$\begin{aligned}\Phi = {} & a_0 + b_0 \log r + c_0 r^2 + d_0 r^2 \log r \\ & + (a_1 r + b_1/r + c_1 r^3 + d_1 r \log r) \cos\theta \\ & + (a'_1 r + b'_1/r + c'_1 r^3 + d'_1 r \log r) \sin\theta \\ & + \sum_{n>2} (a_n r^n + b_n r^{-n} + c_n r^{2+n} + d_n r^{2-n}) \cos n\theta \\ & + \sum_{n>2} (a'_n r^n + b'_n r^{-n} + c'_n r^{2+n} + d'_n r^{2-n}) \sin n\theta \\ & + a_* \theta + b_* r^2 \theta + c_* r\theta \cos\theta + d_* r\theta \sin\theta \end{aligned} \tag{4}$$

Expressions can be deduced for the radial and tangential displacements u_r, u_θ in terms of constants $a_0, b_0, \ldots, d_*$ (ref. 4). Considering symmetry relations (3), all the terms vanish except for a_1, b_1, c_1, d_1, a_n, b_n, c_n, d_n, d_*. Further considerations from relations (1) and (2) imply that only a_1, b_1, c_1, d_1, d_* are to be taken into account, therefore the stress function Φ is reduced to:

$$\Phi = (a_1 r + b_1/r + c_1 r^3 + d_1 r \log r) \cos\theta + d_* r\theta \sin\theta \tag{5}$$

According to reference 3, the displacements are given by

$$2\mu u_r = \{-a_1 + b_1/r^2 + (1-4\nu)c_1 r^2 + d_1[(1-2\nu)\log r - 1]\} \cos\theta + 2d_1\theta(1-\nu)\sin\theta + d_*\{2(1-\nu)\log r \cos\theta + (1-2\nu)\theta \sin\theta\} \quad (6a)$$

$$2\mu u_\theta = \{a_1 + b_1/r^2 + (5-4\nu)c_1 r^2 - d_1(1-2\nu)\log r\}\sin\theta + 2d_1(1-\nu)\theta\cos\theta - \frac{a^*}{r} + d_*[-\sin\theta - 2(1-\nu)\log r \sin\theta + (1-2\nu)\theta\cos\theta] \quad (6b)$$

Where $\mu = \frac{E}{2(1+\nu)}$, the shear modulus.

Enforcing boundary conditions (1) and (2) a system of five equations with five unknowns is obtained:

$$-a_1 + b_1/a^2 + (1-4\nu)c_1 a^2 + d_1[(1-2\nu)\log a - 1] + d_*.2.(1-\nu)\log a = 2\mu\delta$$

$$+a_1 + b_1/a^2 + (5-4\nu)c_1 a^2 - d_1(1-2\nu)\log a - d_*[1+2(1-\nu)\log a] = -2\mu\delta$$

$$-a_1 + b_1/b^2 + (1-4\nu)c_1 b^2 + d_1[(1-2\nu)\log b - 1] + d_* 2(1-\nu)\log b = 0 \quad (7c)$$

$$+a_1 + b_1/b^2 + (5-4\nu)c_1 b^2 - d_1(1-2\nu)\log b - d_*[1 + 2(1-\nu)\log b] = 0 \quad (7d)$$

$$2d_1(1-\nu) + d_*(1-2\nu) = 0 \quad (7e)$$

The solutions of this system are:

$$b_1 = (3-4\nu)c_1 b^2 a^2 \quad (8a)$$

$$d_* = 4(1-\nu)(3-4\nu)c_1(b^2 + a^2) \quad (8b)$$

$$d_1 = -2(1-2\nu)(3-4\nu)c_1(b^2 + a^2) \quad (8c)$$

$$a_1 = c_1[a^2(3-4\nu)^2 + 8b^2(1-\nu)(1-2\nu) - b^2 + 2(3-4\nu)^2(\log b)(a^2 + b^2)] \quad (8d)$$

$$c_1 = \frac{\mu.\delta}{b^2 - a^2 + (3-4\nu)^2(a^2 + b^2) \log (\frac{a}{b})} \quad (8e)$$

A. Relation Between Force and Displacement

The total force F, acting on the rigid cylinder, resulting from its displacement δ, can be obtained by integrating stresses on its surface, or preferably, by using a well-known result of stress functions Φ (ref.4,5) If A and B are extremities of an arc AB on which stresses are acting and $\frac{\partial \Phi}{\partial y}$ is the derivative of Φ with respect to the y ordinate, the resultant of the stresses is given by

$$F = \left(\frac{\partial \Phi}{\partial y} \right)_A^B \quad (9)$$

Here the Γ_1 curve is a closed circuit, A coincides with B; only the non-single valued term of Φ has to be taken into account. Thus

$$F = \left(\frac{\partial \Phi}{\partial y} \right)_0^{2\pi} = 2\pi d_* \quad (10)$$

Therefore by substituting for d_* using (8b) and (8e), we get

$$F = K.\delta \quad (11a)$$

$$K = \frac{8\pi(3-4\nu)(1-\nu)\mu}{\frac{1-(a/b)^2}{1+(a/b)^2} + (3-4\nu)^2 \ln (\frac{a}{b})} \quad (11b)$$

F has dimension of a force per unit length, K has the same dimension as Young's modulus E. It is convenient to introduce the dimensionless quantities $\overline{K}$, $\overline{F}$, $\overline{\delta}$ defined as

$$\overline{K} = \frac{K}{E} \quad ; \qquad \overline{F} = \frac{F}{E \cdot a} \quad ; \qquad \overline{\delta} = \frac{\delta}{a} \tag{12}$$

With this normalization, (11) becomes

$$\overline{F} = \overline{K}\,\overline{\delta} \tag{13a}$$

$$\overline{K} = \frac{4\pi \frac{1-\nu}{1+\nu} (3-4\nu)}{\frac{1-(a/b)^2}{1+(a/b)^2} + (3-4\nu)^2 \ln \left(\frac{a}{b}\right)} \tag{13b}$$

The stiffness $\overline{K}$ versus the ratio $\frac{a}{b}$ has been plotted in Figure 2 for different Poisson's ratio ν. When $\frac{a}{b}$ goes to zero, i.e. when force F is a point load, or where the elastic cylinder is expanded to infinity the $\overline{K}$ value goes to zero with a logarithmic order. When b goes to a, K goes to infinity. This result gives the order of influence on $\overline{K}$ in trying to model an infinite medium by a finite medium. However it does not give a satisfactory stiffness in the case of an infinite elastic medium. This result is apparent in all two-dimensional infinite or semi-infinite elastic problems.

B. Displacement Solution

Introducing a dimensionless quantity ξ defined such that

$$\xi = \frac{r}{a} \tag{14}$$

the displacements u_r, u_θ, at any point of the rigid cylinder are obtained by substituting the values b_1, d_*, d_1, a_1, c_1 in expressions (6a), (6b), and by using ξ:

$$2\mu\, u_r = \{-\bar{a}_1 + \frac{\bar{b}_1}{\xi^2} + (1-4\nu)\bar{c}_1\xi^2 + \bar{d}_1[(1-2\nu)\log\xi - 1] + \bar{d}_*2(1-\nu)\log\xi\}\cos\theta \tag{15a}$$

$$2\mu\, u_\theta = \{\bar{a}_1 + \frac{\bar{b}_1}{\xi^2} + (5-4\nu)\bar{c}_1\xi^2 - \bar{d}_1(1-2\nu)\log\xi - \bar{d}_*[1 + 2(1-\nu)\log\xi]\}\sin\theta \tag{15b}$$

where constants $\bar{a}_1$, $\bar{b}_1$, $\bar{c}_1$, $\bar{d}_1$, $\bar{d}_*$ are defined by:

$$\bar{a}_1 = \bar{c}_1\{(3-4\nu)^2 + 8(\frac{b}{a})^2(1-\nu)(1-2\nu) - (\frac{b}{a})^2 + 2(3-4\nu)^2[1 + (\frac{b}{a})^2]\log(\frac{b}{a})\} \tag{16a}$$

$$\bar{d}_1 = -2(1-2\nu)(3-4\nu)\bar{c}_1\left(1 + \frac{b^2}{a^2}\right) \tag{16b}$$

$$\bar{d}_* = \pm 4(1-\nu)(3-4\nu)\bar{c}_1\left(1 + \frac{b^2}{a^2}\right) \tag{16c}$$

$$\bar{b}_1 = (3-4\nu)\bar{c}_1\frac{b^2}{a^2} \tag{16d}$$

$$\bar{c}_1 = \frac{\mu\cdot\delta}{\frac{b^2}{a^2} - 1 + (3-4\nu)^2\left(\frac{b^2}{a^2} + 1\right)\log\frac{a}{b}} \tag{16e}$$

The displacements can be also expressed in terms of applied load F, using relation (11b)

$$\bar{c}_1 = \frac{F}{8\pi(1-\nu)(3-4\nu)\{1 + (\frac{b}{a})^2\}} \tag{17}$$

The displacements satisfy the boundary conditions.

C. Stress Solution and Stress Limit in Case of an Infinite Medium

The stresses in polar coordinates are obtained from the stress function Φ:

$$\sigma_r = \frac{1}{r}\frac{\partial \Phi}{\partial r} + \frac{1}{r^2}\frac{\partial^2 \Phi}{\partial \theta^2} \tag{18a}$$

$$\sigma_\theta = \frac{\partial^2 \phi}{\partial \theta^2} \tag{18b}$$

$$\sigma_{r\theta} = -\frac{\partial}{\partial r}\left(\frac{1}{r}\frac{\partial \Phi}{\partial \theta}\right) \tag{18c}$$

Substituting Φ given in relation (5), using relations (8), the stresses in terms of displacements or in terms of applied load are

$$\sigma_r = 2(\bar{c}_1/a)\{-(3-4\nu)\frac{(a/b)^2}{\xi^3} + \xi + [1 + (\frac{a}{b})^2](3-4\nu)(3-2\nu)\frac{1}{\xi}\} \tag{19a}$$

$$\sigma_\theta = 2(\bar{c}_1/a)\{+(3-4\nu)\frac{(a/b)^2}{\xi^3} + 3\xi + [1 + (\frac{a}{b})^2](3-4\nu)(1-2\nu)\frac{1}{\xi}\} \tag{19b}$$

$$\sigma_{r\theta} = 2(\bar{c}_1/a)\{-(3-4\nu)\frac{(a/b)^2}{\xi^3} + \xi - [1 + (\frac{a}{b})^2](3-4\nu)(1-2\nu)\frac{1}{\xi}\} \tag{19c}$$

where $\bar{c}_1$ is given by (16e) or (17).

When the elastic domain is expanded to infinity, i.e. when $a/b \to 0$, a stress limit exists; introducing the dimensionless quantities $\bar{\sigma}_r$, $\bar{\sigma}_\theta$, $\bar{\sigma}_{r\theta}$ where

$$\bar{\sigma}_r = \frac{\sigma_r \cdot a}{F} \quad , \quad \bar{\sigma}_\theta = \frac{\sigma_\theta \cdot a}{F} \quad , \quad \bar{\sigma}_{r\theta} = \frac{\sigma_{r\theta} \cdot a}{F} \tag{20}$$

the limit of stress is expressed as follows:

$$\bar{\sigma}_r = + \frac{\cos\theta}{4\pi(1-\nu)\xi}\{+\frac{1}{\xi^2} - 3 + 2\nu\} \tag{21a}$$

$$\bar{\sigma}_\theta = \frac{\cos\theta}{4\pi(1-\nu)\xi}\{-\frac{1}{\xi^2} + 1 - 2\nu\} \tag{21b}$$

$$\bar{\sigma}_{r\theta} = \frac{\sin\theta}{4\pi(1-\nu)\xi}\{+\frac{1}{\xi^2} + 1 - 2\nu\} \tag{21c}$$

In particular on the rigid cylinder the stresses are obtained by setting $\xi = 1$, so that

$$\bar{\sigma}_r(a) = \frac{\cos\theta}{2\pi} \tag{22a}$$

$$\bar{\sigma}_\theta(a) = -\frac{\cos\theta}{2\pi}\frac{\nu}{1-\nu} \tag{22b}$$

$$\bar{\sigma}_{r\theta}(a) = +\frac{\sin\theta}{2\pi} \tag{22c}$$

IV. RESULTS AND PRACTICAL APPLICATIONS

For numerical calculations, three different values of Poisson's ratio have been selected: two extreme 0 and 0.5 and an intermediate value 0.3 as a commonly used value for soils. A Poisson's ratio equal to 0.5 could be considered in connection with undrained conditions.

Three different points have been investigated:

- stress distribution in the elastic medium
- stress distribution on the rigid cylinder
- initiation of plasticity in the elastic domain.

A. Stress Distribution in an Elastic Medium

Normalized stresses given by relations (21) have been plotted for angles $\theta = 0$ and $\theta = \frac{\pi}{2}$, i.e. along x- and y-axes in Figures 3 and 4. Shear stress $\bar{\sigma}_{r\theta}$ along x axis is zero according to presence of sin θ in (21c); along y-axis, both $\bar{\sigma}_r$ and $\bar{\sigma}_\theta$ are zero.

Along x-axis $\bar{\sigma}_r$ exhibits a peak except when $\nu = 0$. This maximum could be explained by a combination of the effects of a displacement boundary condition and Poisson's ratio effect in the neighborhood of the cylinder. All the stresses go to zero at infinity. A magnification of stress pattern in the elastic medium has been represented in Figure 5 using iso-principal stress contours: on each line, the normalized principal stress $\bar{\sigma}_1$, $\bar{\sigma}_3$ are constant and equal to the indicated values.

B. Stress Distribution on Rigid Cylinder

The stresses given in relation (22) and the corresponding normalized principal stresses $\bar{\sigma}_1^{(a)}$, $\bar{\sigma}_3^{(a)}$ have been plotted in Fig. 6 and 7 versus angle θ. It is noticed that $\bar{\sigma}_r^{(a)}$ and $\bar{\sigma}_{r\theta}^{(a)}$ do not depend on Poisson's ratio. The maximum shear stress occurs at $\theta = \frac{\pi}{2}$ and has the following value.

$$\bar{\sigma}_{r\theta}^{(a)} = \frac{\sigma_{r\theta\ (a)} \cdot a}{F} = \frac{1}{2\pi} \qquad (23)$$

For $\nu = 0.5$, $\bar{\sigma}_r^{(a)}$ and $\bar{\sigma}_\theta^{(a)}$ are equal.

C. Plasticity Initiation (Elastic Domain)

In order to predict when and where plastic regions are initiated in the elastic medium, two classical failure criteria in soil mechanics have been selected: Von Mises and Mohr-Coulomb.

1. Cohesive Material (Von Mises)

Plasticity begins when the deviator stress defined as the difference of principal stresses σ_1, σ_3 becomes equal to twice the material cohesion, usually denoted c. The normalized deviator stress $(\bar{\sigma}_1 - \bar{\sigma}_3)$, which could be defined as in relations (20), has been plotted on the rigid cylinder versus angle Θ for different Poisson's ratios in Figure 8 and in the elastic medium in the particular case of incompressibility (Fig. 9). The maximum deviator stress, independent of Poisson's ratio is equal to $1/\pi$ for an angle equal to $\pi/2$. This allows us to define a limiting elastic domain in which the applied load F is just equal to $F_{plastic}$ where

$$F_{plastic} = 2ca\pi \tag{24}$$

2. Cohesionless Material. (Mohr-Coulomb)

For a cohesionless material, an initial compression stress is necessary in order to prevent $\sigma_r + \sigma_\theta$ from becoming zero for $\theta = \frac{\pi}{2}$, which would give an infinite value to sin ϕ. sin ϕ has been defined as

$$\sin \phi = \frac{| \sigma_1 - \sigma_3 |}{| \sigma_r + \sigma_\theta |} \tag{25}$$

Consequently, an isotropic compressive pressure σ_0 has been introduced

$$\sigma_r = \sigma_\theta = \sigma_0 \tag{26}$$

after normalization as in relation (20)

$$\bar{\sigma}_0 = \frac{\sigma_0 \cdot a}{F} \tag{27}$$

The value of $\bar{\sigma}_0$ for the beginning of plasticity is shown in Fig. 10. This figure gives the values F, a, σ_0 at which plasticity is initiated. The value of $\bar{\sigma}_0$ has been obtained by noticing that plasticity occurs first at the cylinder and by fixing the maximum value sin [ϕ_{failure}] at that point

$$\bar{\sigma}_0 = -\left(\frac{1}{\sin^2 \phi} + \frac{1}{3-4\nu}\right)^{\frac{1}{2}} \frac{1}{2\pi} = \frac{\sigma_0 a}{F} \tag{28}$$

Plasticity is initiated at an angle β which depends on Poisson's ratio and ϕ_{failure}. This angle β is given by the following relation, (29), and has been plotted in Figure 11:

$$\cos \beta = -\frac{2(1-\nu)}{(3-4\nu)\left(\frac{1}{\sin^2 \phi} + \frac{1}{3-4\nu}\right)^{\frac{1}{2}}} \tag{29}$$

It is noticeable that plasticity is no longer initiated for $\theta = \frac{\pi}{2}$ but for θ larger than $\frac{\pi}{2}$. The ratio $\frac{\sin \phi}{\sin \phi_{\text{failure}}}$ on the rigid cylinder has been plotted in Figure 12, and sin ϕ in the elastic medium has been plotted in figure 13 for the particular case of $\nu = 0.3$ and $\phi_{\text{failure}} = 45°$.

V. CONCLUSION

An analytical solution has been presented for the problem of a rigid cylinder displaced laterally in an elastic medium. Using these solutions, the stresses have been investigated in the elastic region and more intensively on the cylindrical surface. The development of a plastic region has been examined for cohesive and cohesionless materials. A force displacement relation taking into account the elastic medium size has been proposed; its validity domain is also mentioned. It was found that the size of the elastic medium has very little influence on the stresses adjacent to the cylinder but is all-important for the overall stiffness K.

These results can be applied not only to problems of lateral loading on piles and piers but also in the case of buckling of underground pipelines and other situations where rigid cylinders embedded in elastic media are subjected to lateral loads.

I. ACKNOWLEDGEMENT

The author wishes to thank Professor E.Sternberg for valuable discussions on the subject.

VII. REFERENCES

1. F.Baguelin, R.Frauck and Y.H.Said, "Theoretical Study of Lateral Reaction Mechanism of piles", Geotechnique 27 No.3, 1977, 405-434.

2. E.G.Coker and L.N.G.Filon, A Treatise on Photoelasticity, Cambridge University Press, 1931.

3. R.E.Gibson and W.F.Anderson, "In-Situ Measurement of Soil Properties with the Pressuremeter", Civil Engineering and Public Works Review, Rev.56, No.658, 615-618.

4. W. Flügge, ed., Handbook of Engineering Mechanics, Chapter 37, McGraw-Hill, New York, 1962.

5. S.P.Timoshenko and J.N.Goodier, Theory of Elasticity, Engineering Societies Monographs, Third Edition, McGraw Hill, 1970.

FIGURE CAPTIONS

1 Domain of the problem

2 Global stiffness of elastic medium $\bar{K}$ versus the ratio a/b for different Poisson's ratio

3 Stresses $\bar{\sigma}_{rr}$, $\bar{\sigma}_{\theta\theta}$ along x axis for different Poisson's ratio

4 Stress $\bar{\sigma}_{r\theta}$ along y axis for different Poisson's ratio

5 Iso-principal stress contours in the elastic medium for $\nu = 0.3$

6 Stress distribution on the rigid cylinder

7 Principal stress values on the rigid cylinder

8 Deviator stress on cylinder versus angle θ

9 Deviator stress in elastic medium for $\nu = 0.5$

10 Initial compressive isotropic stress σ_0 and applied lateral load F at initiation of plasticity for a cohensionless material with different Poisson's ratio ν and friction angle $\phi_{failure}$

11 Location of plasticity for a cohesionless material with different Poisson's ratio and friction angle

12 $\sin \phi / \sin \phi_{failure}$ at initiation of plasticity on the rigid cylinder for a cohesionless material

13 $\sin \phi$ at initiation of plasticity in an elastic cohesionless material, $\phi_{failure} = 45°$, $\nu = 0.3$

NOTATIONS

Φ	stress function
u_r, u_θ	radial, tangential displacement.
r, θ	polar coordinates
δ	horizontal displacement of rigid cylinder
E, ν	Young's Modulus and Poisson's Ratio of elastic medium
$\mu = \frac{E}{2(1+\nu)}$	shear modulus
a_0, b_0, c_0, d_0 $a_1 b_1$, $c_1 d_1$ a_*, b_*, c_*, d_*	constant of stress function Φ
$\sigma_r, \sigma_\theta, \sigma_{r\theta}$	radial, tangential and shear stress
σ_1, σ_3	maximium and minimum principal stresses
a, b	inner and outer radius of elastic medium
ξ	normalized distance $\frac{r}{a}$
F	horizontal applied load on rigid cylinder
$\phi_{failure}$, ϕ_f	friction angle
c	cohesion
$K, \bar{K}$	stiffness and normalized stiffness defined by $F = K\delta$ and $\bar{K} = K/E$
$\bar{a}_1, \bar{b}_1, \bar{c}_1, \bar{d}_1$	constant associated with normalized distance δ
$\bar{\sigma}_r, \bar{\sigma}_\theta, \bar{\sigma}_{r\theta}, \bar{\sigma}_1, \bar{\sigma}_3$	normalized stresses

TABLE 1: Values of Principal Stress in Figure 5: $\nu = 0.3$, Infinite Medium

A	-0.068	L	-0.198
B	-0.041	M	-0.171
C	-0.015	N	-0.145
D	+0.012	O	-0.118
E	+0.038	P	-0.092
F	+0.065	Q	-0.065
G	+0.092	R	-0.038
H	+0.118	S	-0.012
I	+0.145	T	+0.015
J	+0.171	U	+0.041
K	+0.198	V	+0.068

TABLE 2: Values of Deviatoric Stress in Figure 9: $\nu = 0.5$ Infinite Medium

A	0.0	G	0.191
B	0.032	H	0.223
C	0.064	I	0.255
D	0.095	J	0.286
E	0.127	K	0.318
F	0.159		

TABLE 3: Values of sin ϕ in Figure 13: $\nu = 0.3$ $\phi_{failure} = 4.5°$ Infinite Medium

A	0.0	G	0.424
B	0.071	H	0.495
C	0.141	I	0.566
D	0.212	J	0.636
E	0.282	K	0.706
F	0.353		

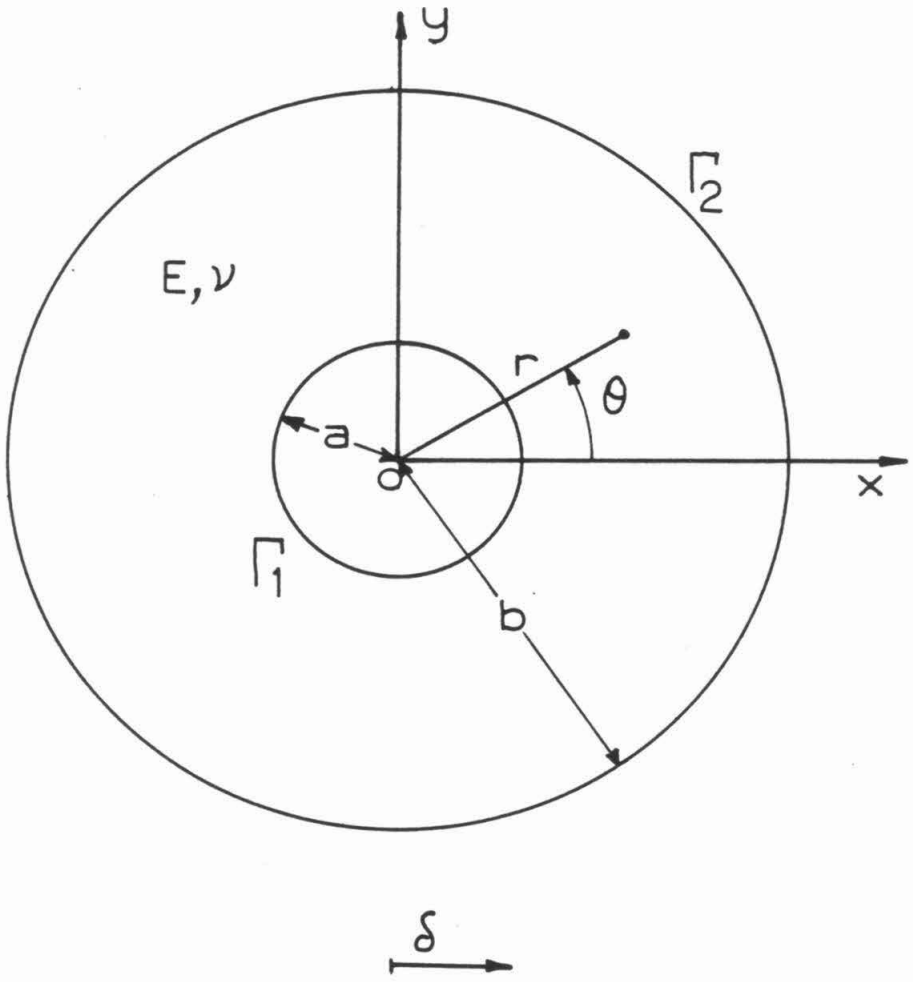

Fig. 1

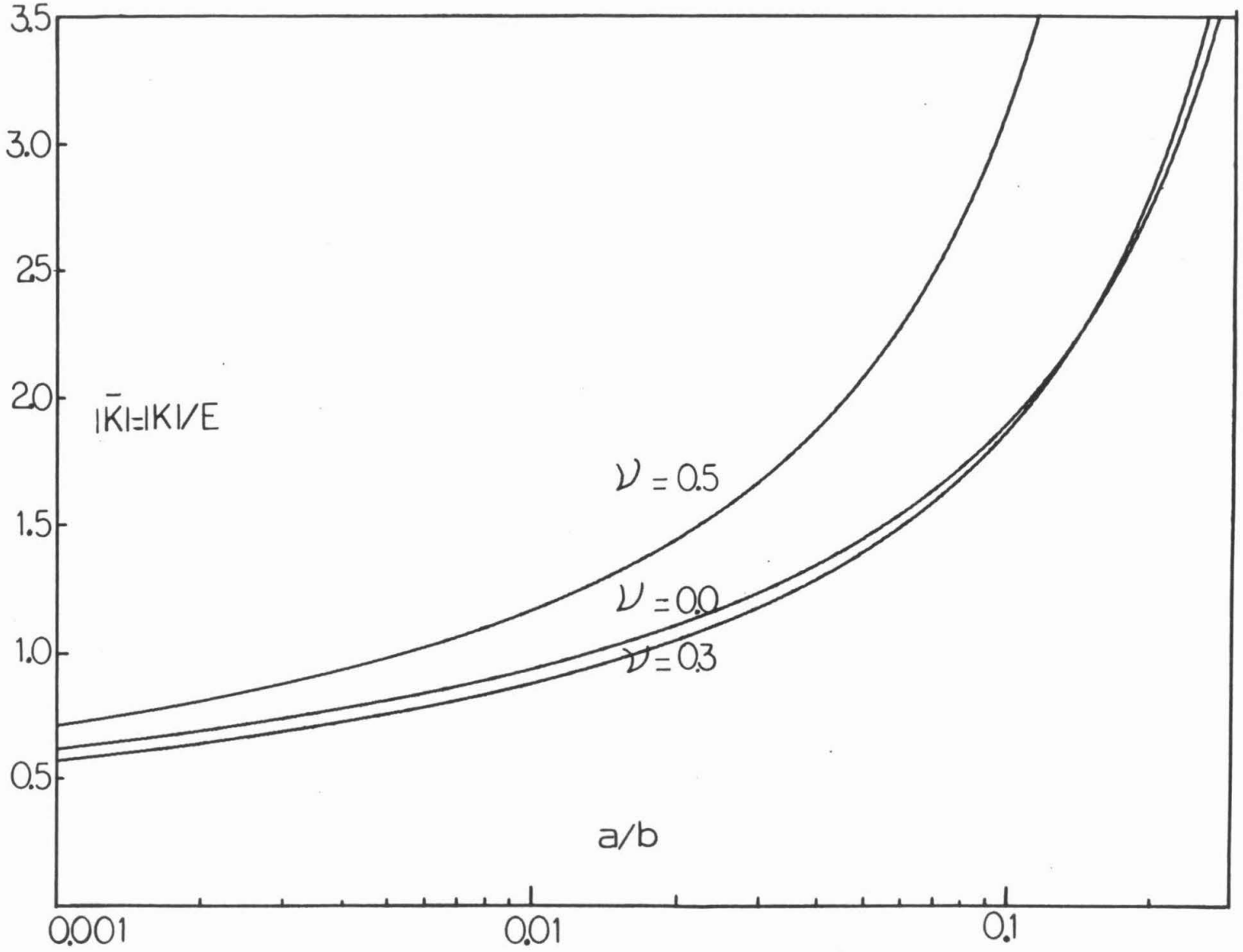

Fig. 2

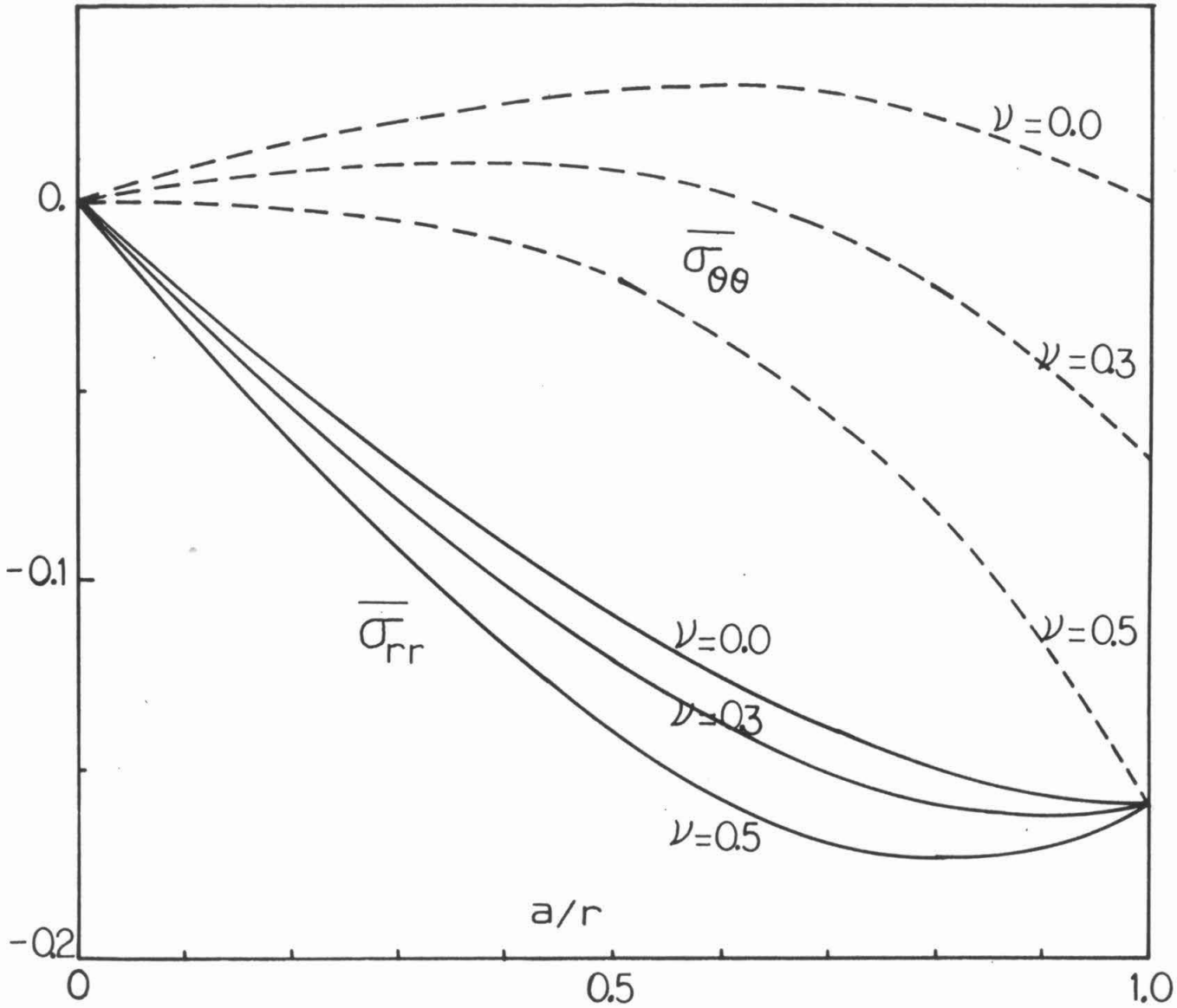
0.
-0.1
-0.2
0
0.5
1.0
a/r
$\overline{\sigma}_{\theta\theta}$
$\overline{\sigma}_{rr}$
$\nu = 0.0$
$\nu = 0.3$
$\nu = 0.5$
$\nu = 0.0$
$\nu = 0.3$
$\nu = 0.5$

Fig. 3

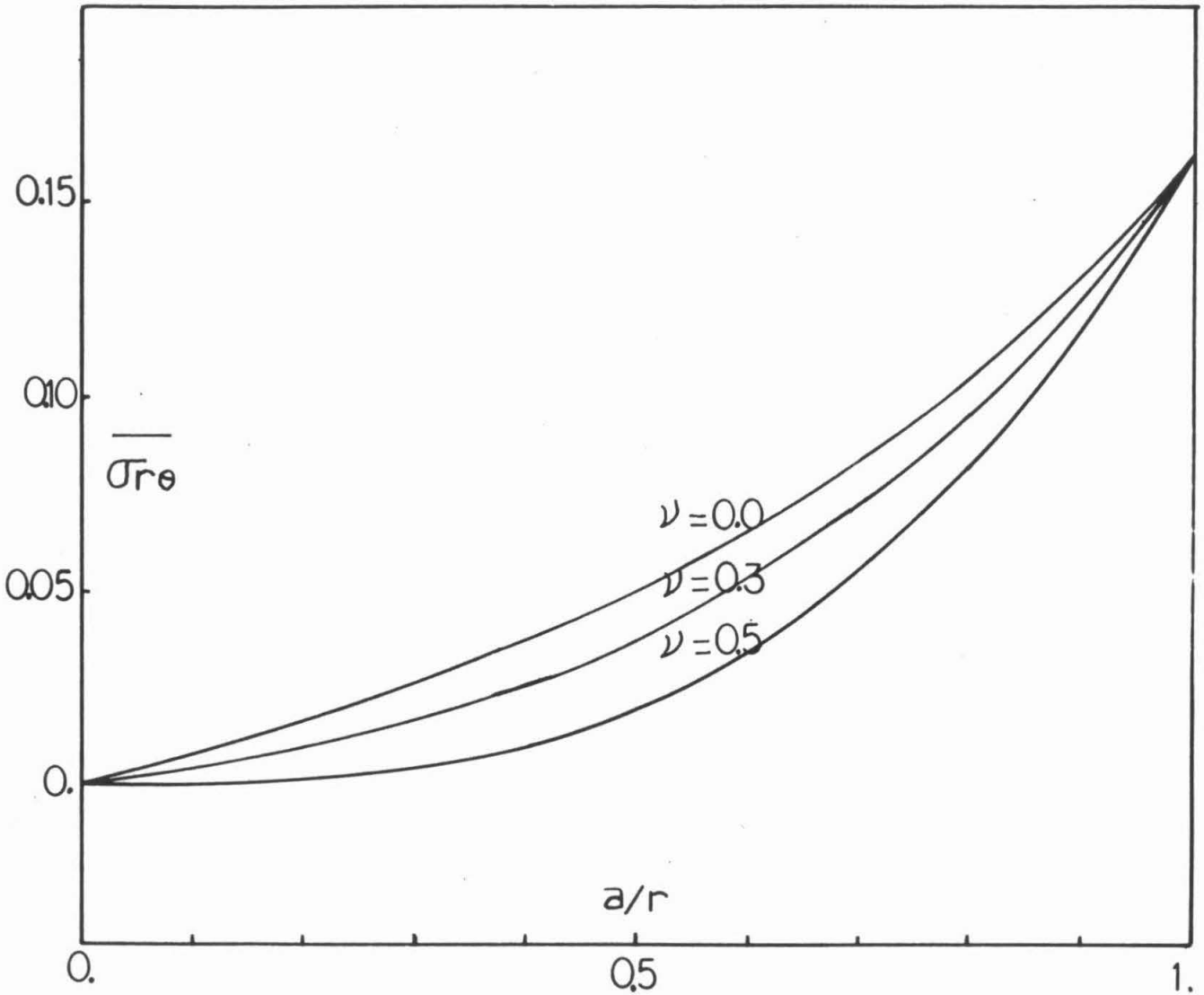

Fig. 4

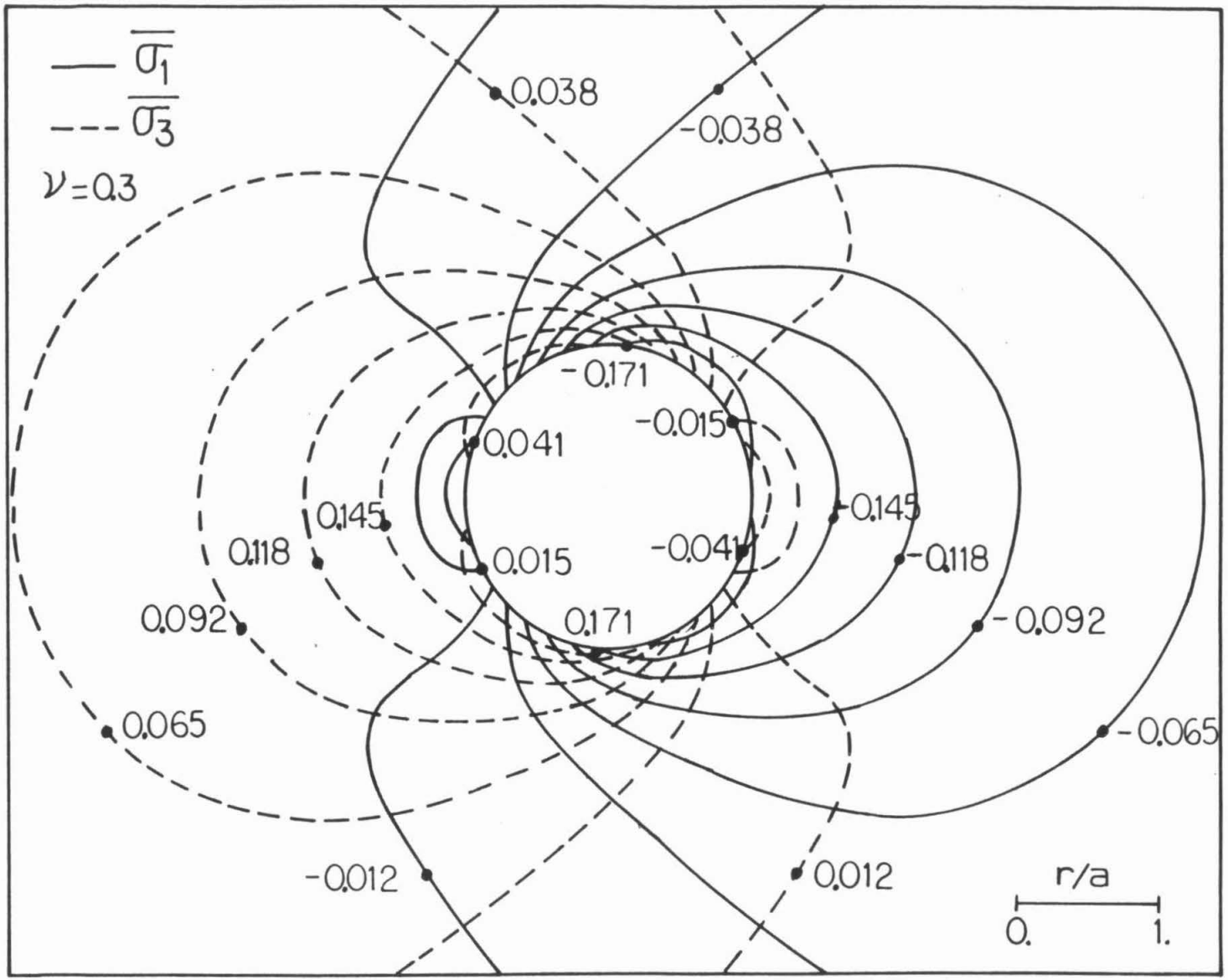
$\overline{\sigma_1}$
$\overline{\sigma_3}$
$\nu = 0.3$
0.038
-0.038
-0.171
-0.015
0.041
0.145
0.118
0.015
-0.041
0.171
0.092
0.065
-0.012
0.012
-0.145
-0.118
-0.092
-0.065
r/a
0.
1.

Fig. 5

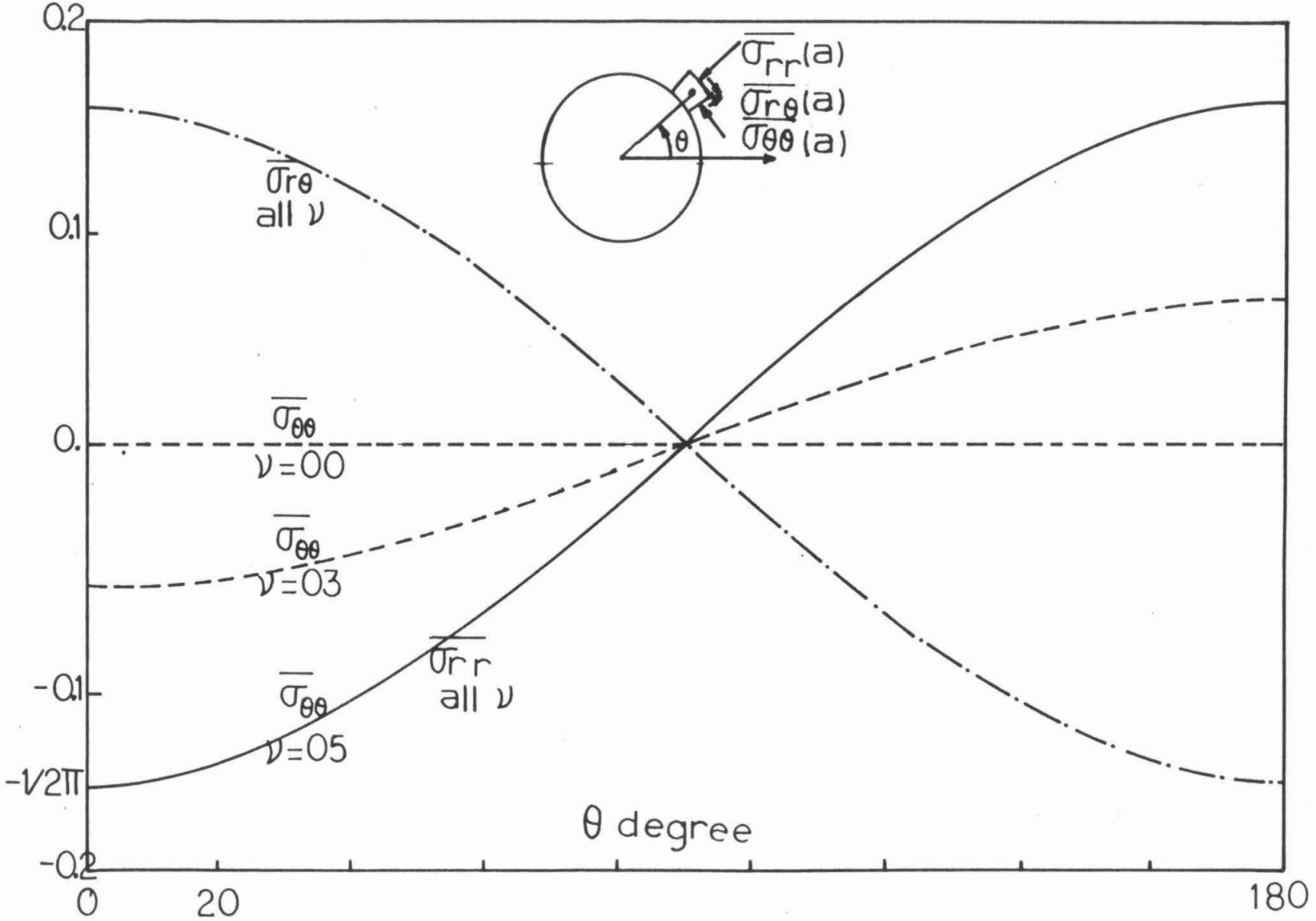
0.2
0.1
0.
-0.1
-1/2π
-0.2
0
20
180
θ degree
$\overline{\sigma_{rr}}$(a)
$\overline{\sigma_{r\theta}}$(a)
$\overline{\sigma_{\theta\theta}}$(a)
θ
$\overline{\sigma_{r\theta}}$ all ν
$\overline{\sigma_{\theta\theta}}$ ν=00
$\overline{\sigma_{\theta\theta}}$ ν=03
$\overline{\sigma_{\theta\theta}}$ ν=05
$\overline{\sigma_{rr}}$ all ν

Fig. 6

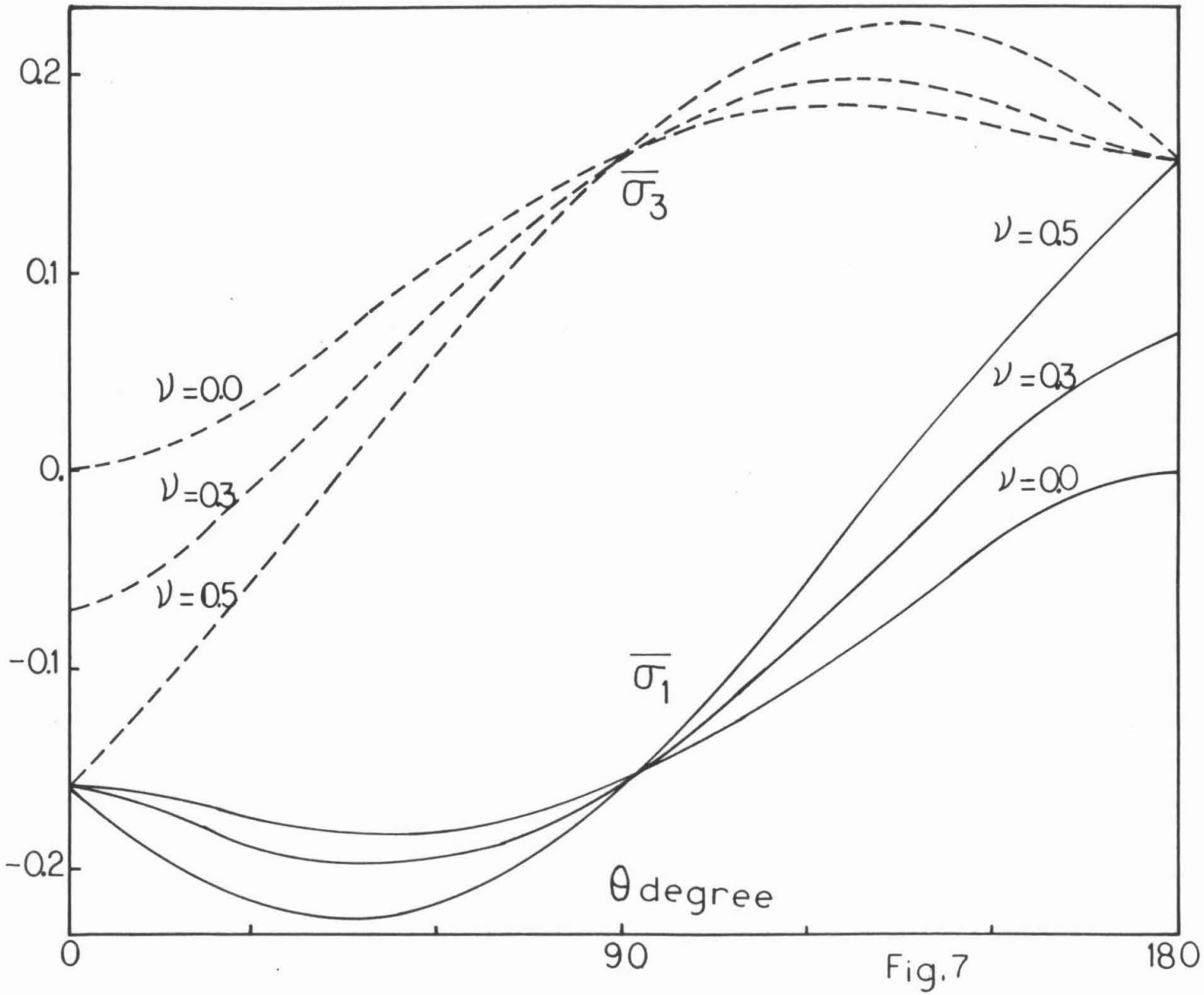
0.2
0.1
0.
-0.1
-0.2
0
90
180
θ degree
$\overline{\sigma_3}$
$\overline{\sigma_1}$
ν = 0.0
ν = 0.3
ν = 0.5
ν = 0.5
ν = 0.3
ν = 0.0

Fig. 7

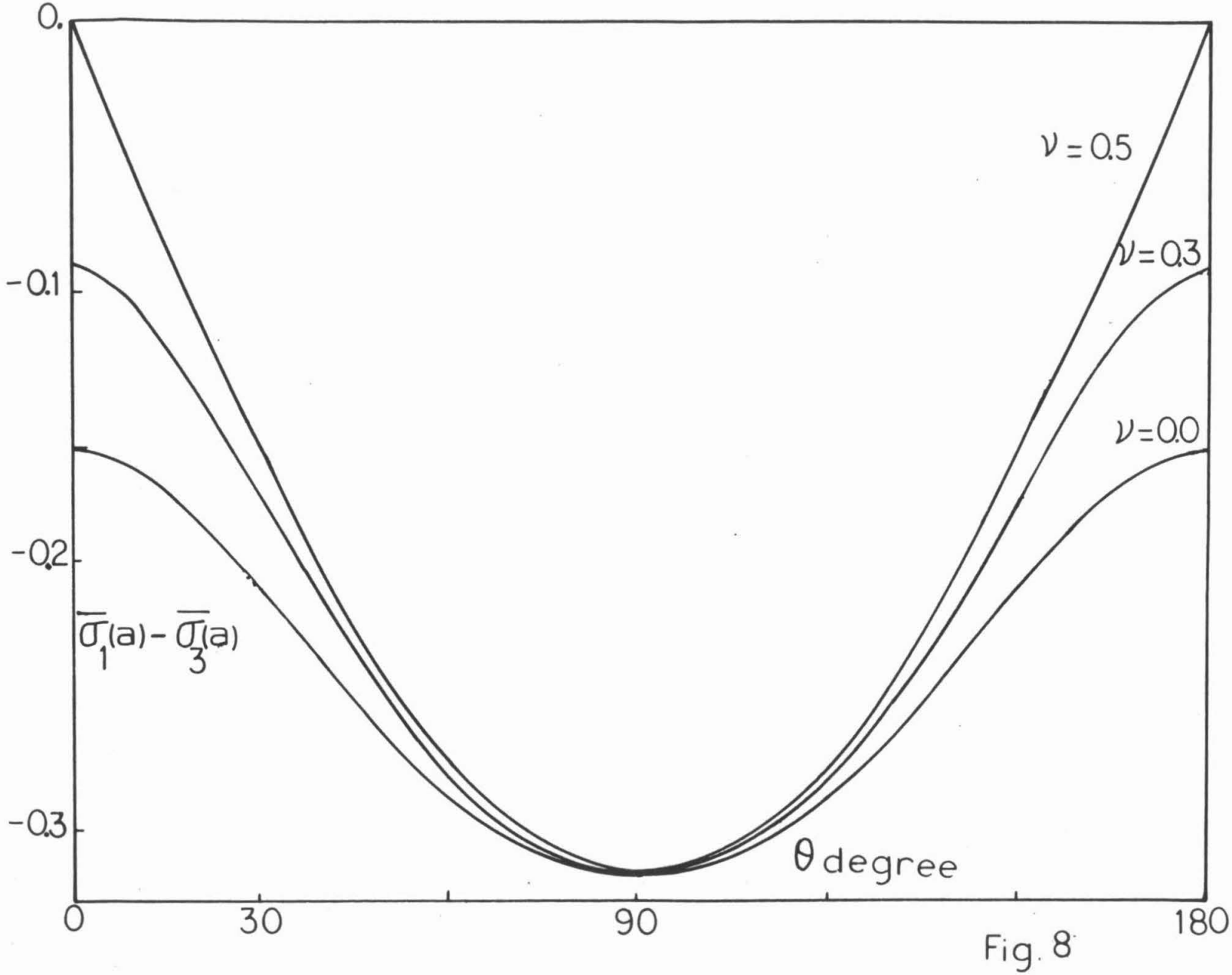
0.
-0.1
-0.2
-0.3
$\nu = 0.5$
$\nu = 0.3$
$\nu = 0.0$
$\overline{\sigma}_1(a) - \overline{\sigma}_3(a)$
θ degree
0
30
90
180

Fig. 8

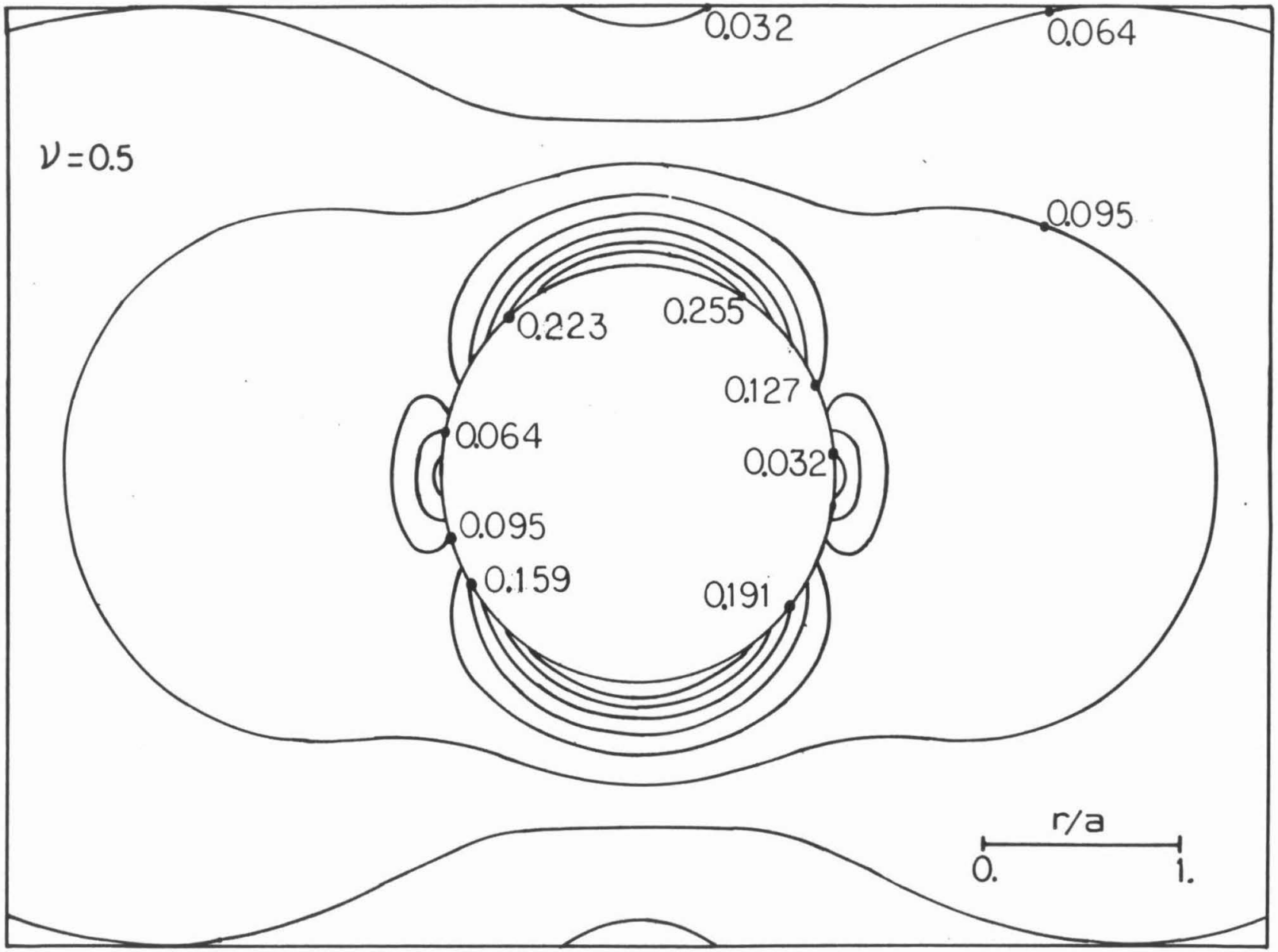
0.032
0.064
ν = 0.5
0.095
0.223
0.255
0.127
0.064
0.032
0.095
0.159
0.191
r/a
0.
1.

Fig. 9

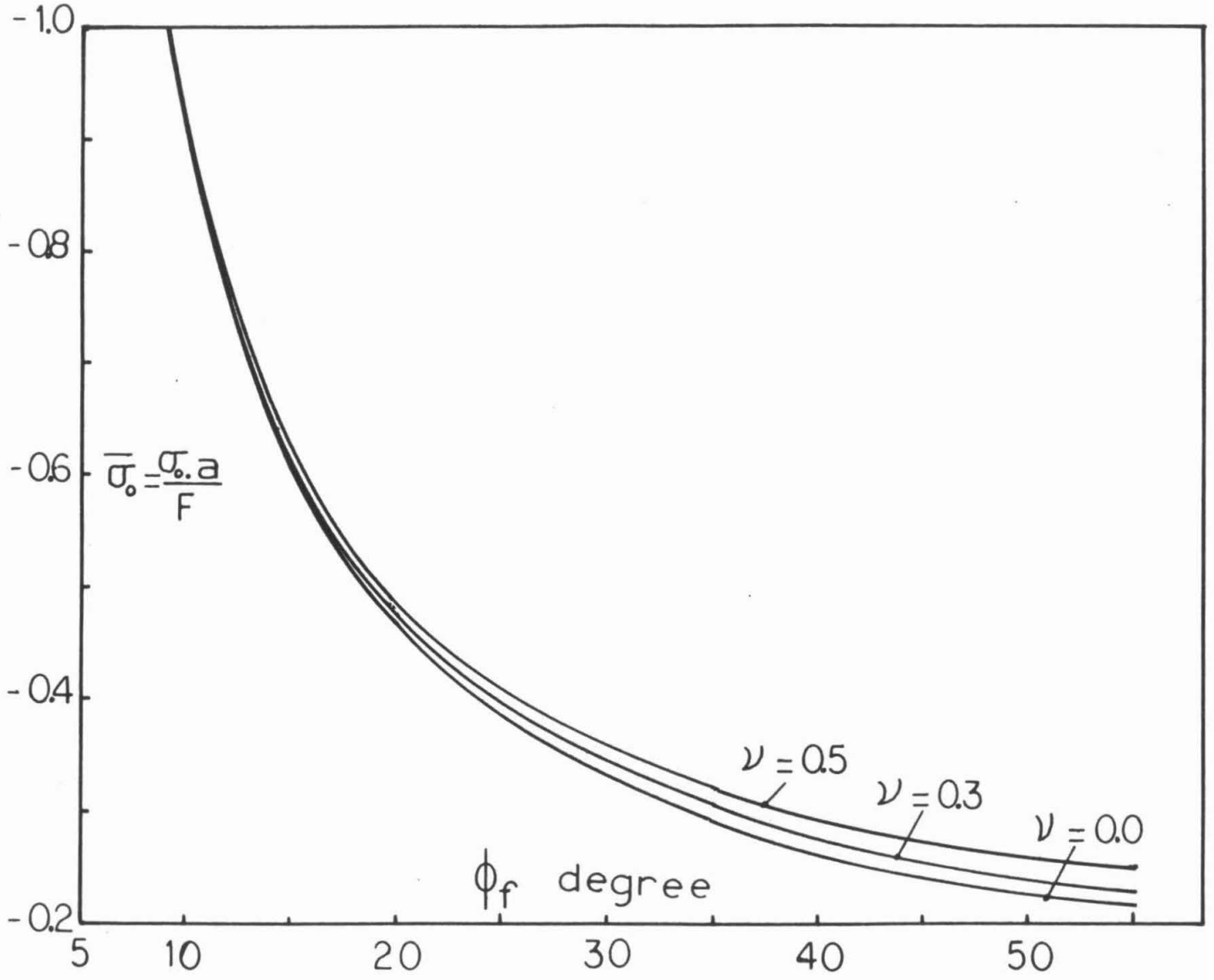
-1.0
-0.8
-0.6
-0.4
-0.2
$\bar{\sigma}_o = \frac{\sigma_o . a}{F}$
$\nu = 0.5$
$\nu = 0.3$
$\nu = 0.0$
ϕ_f degree
5
10
20
30
40
50

Fig. 10

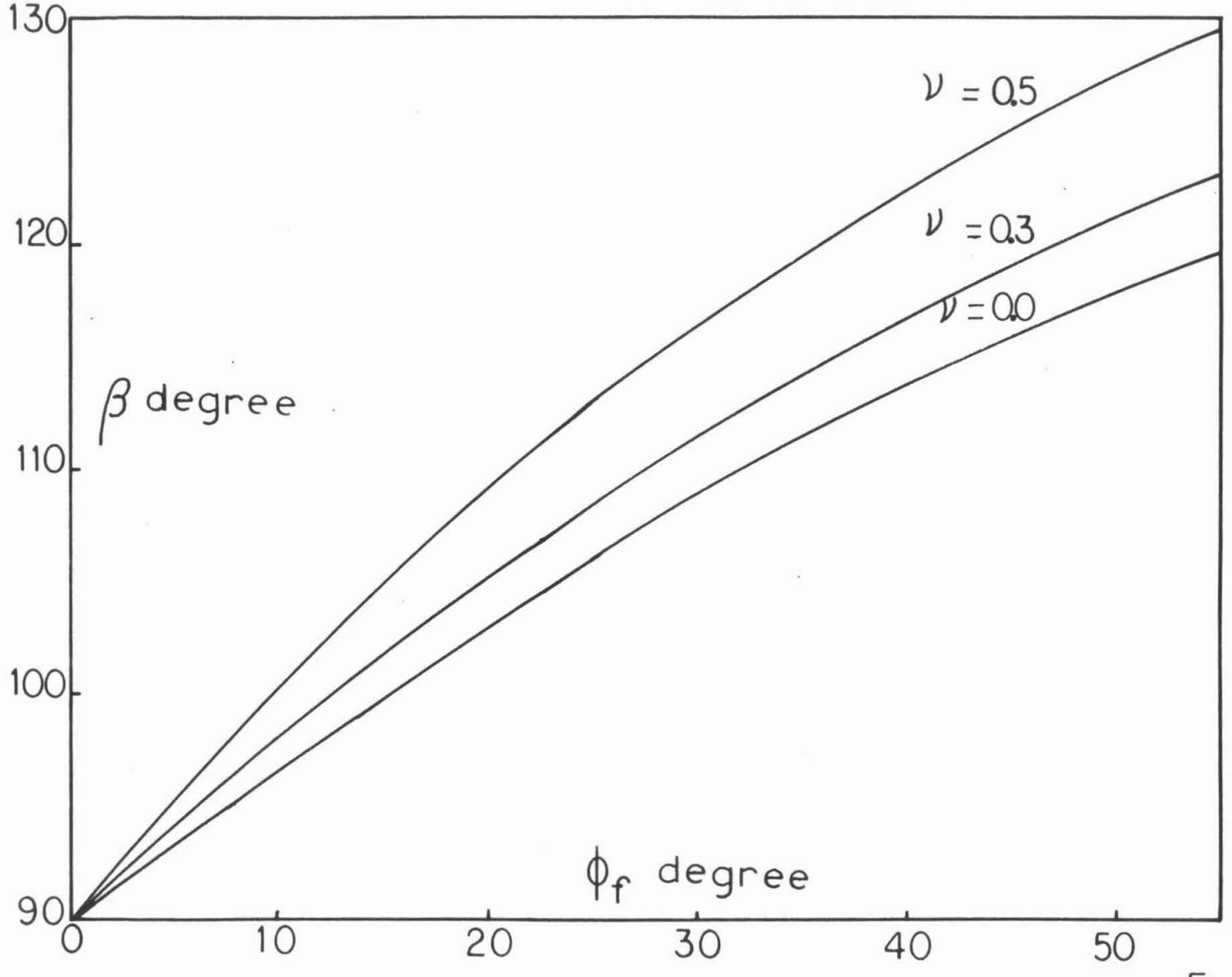
130
120
110
100
90
0
10
20
30
40
50
β degree
ϕ_f degree
ν = 0.5
ν = 0.3
ν = 0.0

Fig. 11

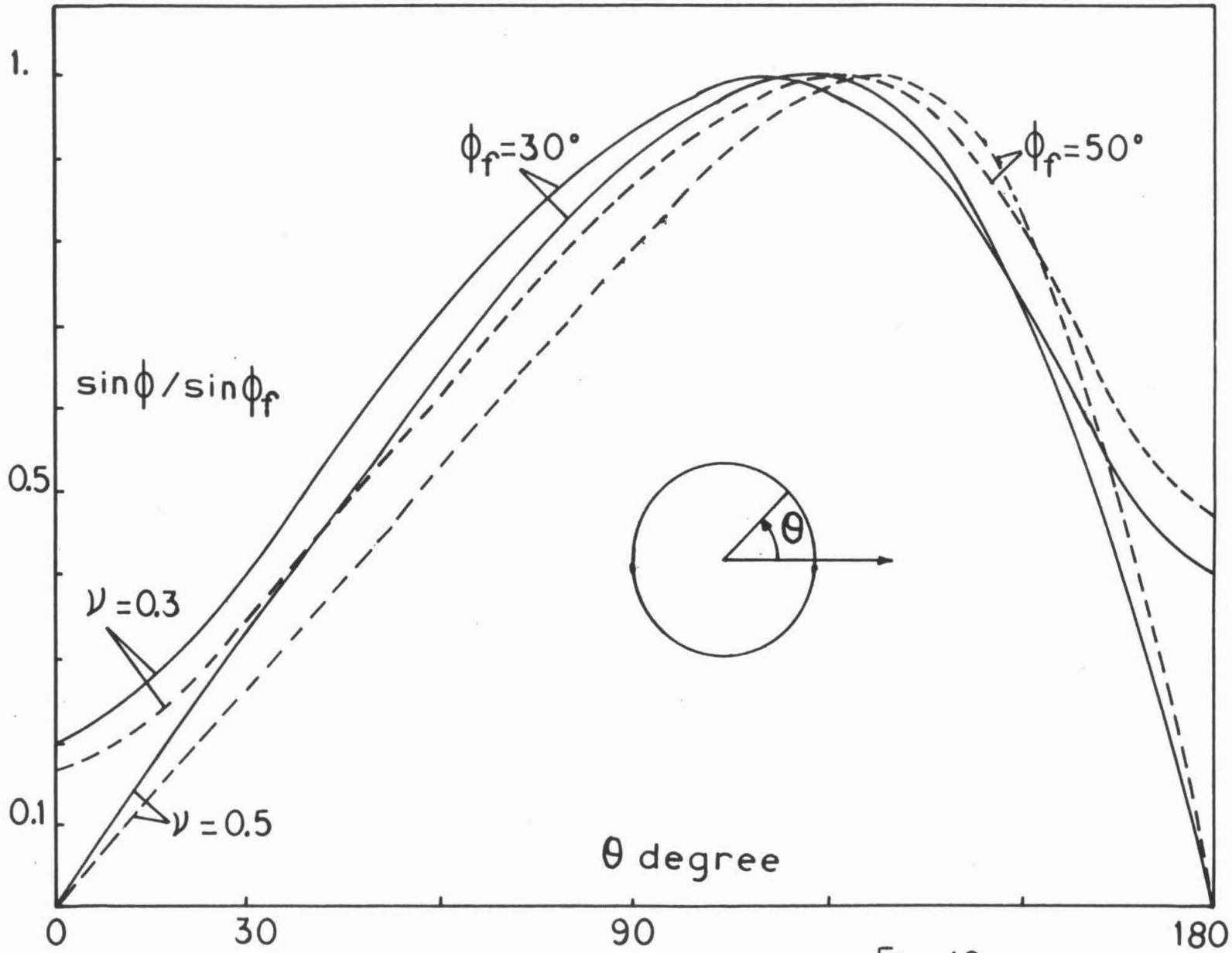
1.
0.5
0.1
$\sin\phi/\sin\phi_f$
ϕ_f=30°
ϕ_f=50°
ν=0.3
ν=0.5
θ
θ degree
0
30
90
180

Fig. 12

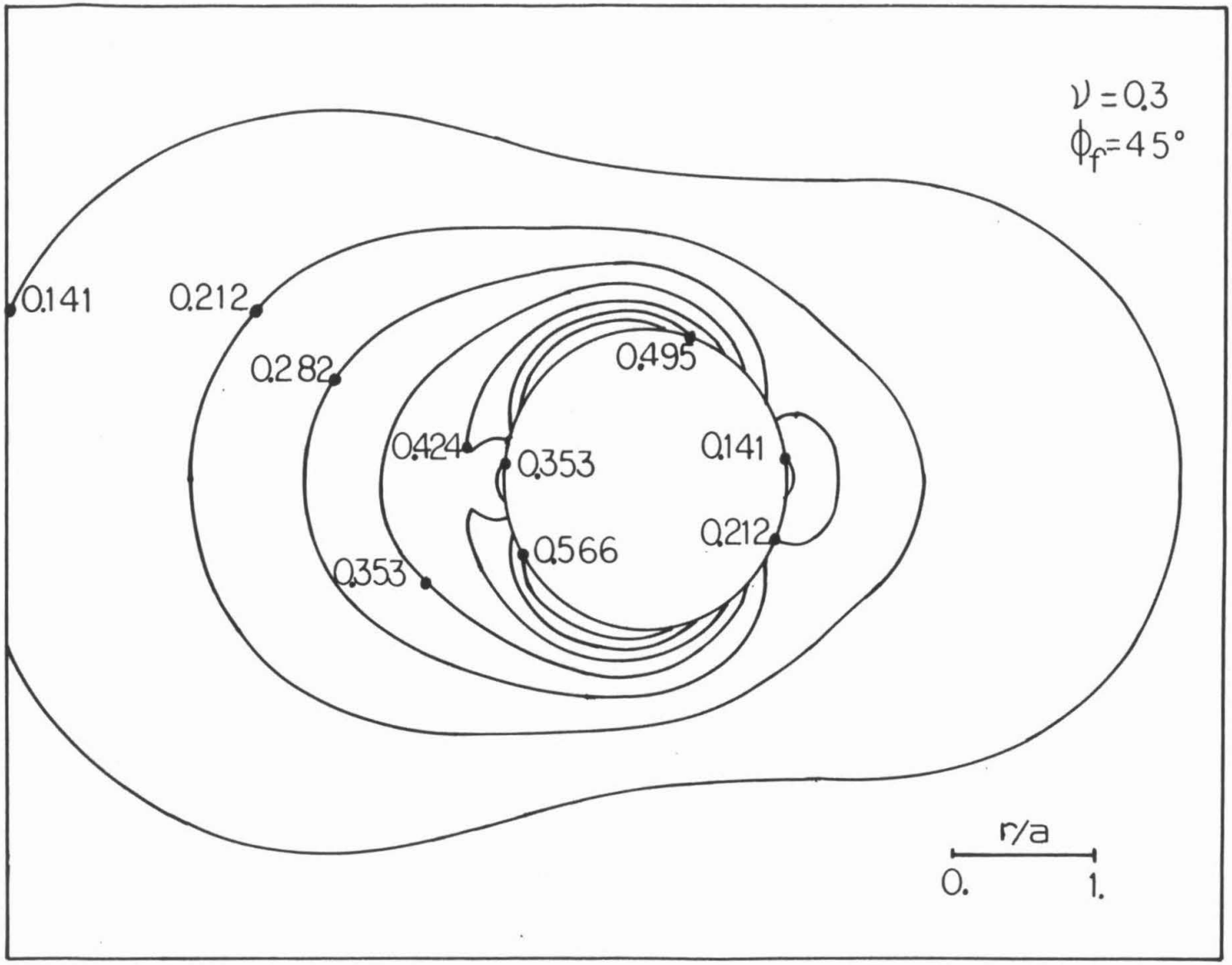
ν = 0.3
ϕ_f = 45°
0.141
0.212
0.282
0.495
0.424
0.353
0.141
0.212
0.566
0.353
r/a
0.
1.

Fig. 13